AD-A053 308 NAVAL RESEARCH LAB WASHINGTON D C F/G 20/12
CHARACTERIZATION OF III-V MATERIALS. ANNUAL SUMMARY REPORT, 1 O--ETC(U)
FEB 78 B D MCCOMBE
UNCLASSIFIED NRL-MR-3701 NL

1 OF 2
AD A053308

NRL Memorandum Report 3701

Characterization of III-V Materials

Annual Summary Report
1 October 1976 to 30 September 1977

BRUCE D. MCCOMBE

Semiconductors Branch
Electronics Technology Division

February 1978

NAVAL RESEARCH LABORATORY
Washington, D.C.

SECURITY CLASSIFICATION OF THIS PAGE (When Data Entered)

REPORT DOCUMENTATION PAGE

READ INSTRUCTIONS BEFORE COMPLETING FORM

1. REPORT NUMBER
NRL Memorandum Report 3701

2. GOVT ACCESSION NO. (14) NRL-MR-3701

3. RECIPIENT'S CATALOG NUMBER

4. TITLE (and Subtitle)
(6) CHARACTERIZATION OF III-V MATERIALS
ANNUAL SUMMARY REPORT
1 October 1976 to 30 September 1977

5. TYPE OF REPORT & PERIOD COVERED
Summary report on an NRL problem.

6. PERFORMING ORG. REPORT NUMBER

7. AUTHOR(s)
(10) Bruce D. McCombe, Editor

8. CONTRACT OR GRANT NUMBER(s)
(16) F54582
(17) RF54582001
RF54582-001

9. PERFORMING ORGANIZATION NAME AND ADDRESS
Naval Research Laboratory
Washington, D.C. 20375

10. PROGRAM ELEMENT, PROJECT, TASK AREA & WORK UNIT NUMBERS
NRL Problem P01-14

11. CONTROLLING OFFICE NAME AND ADDRESS
Office of Naval Research
Electronics Program Office
Arlington, Virginia 22217

12. REPORT DATE
(11) Feb[illegible]78

13. NUMBER OF PAGES
(12) 109 p.
108

14. MONITORING AGENCY NAME & ADDRESS(if different from Controlling Office)

15. SECURITY CLASS. (of this report)
UNCLASSIFIED

15a. DECLASSIFICATION/DOWNGRADING SCHEDULE

16. DISTRIBUTION STATEMENT (of this Report)

Approved for public release; distribution unlimited.

17. DISTRIBUTION STATEMENT (of the abstract entered in Block 20, if different from Report)

18. SUPPLEMENTARY NOTES

19. KEY WORDS (Continue on reverse side if necessary and identify by block number)

Semi-insulating gallium arsenide	Photovoltaic	Mobility
Characterization	Photoelectromagnetic	Carrier density
Epitaxial	Galvanomagnetic	Photoluminescence excitation
Photoconductivity	Van der Pauw	Field effect transistor
Contactless	Infrared reflectance	Schottky barrier

20. ABSTRACT (Continue on reverse side if necessary and identify by block number)

A program for the characterization of bulk and epitaxial single crystals of III-V compounds is described. The program includes electrical, chemical, structural and topographic characterization as well as device fabrication and evaluation, and is carried out on a co-ordinated basis by three Navy laboratories: The Naval Research Laboratory, the Naval Surface Weapons Center, and the Naval Ocean Systems Center. The primary goals of the effort continue to be: (1) To provide rapid and interactive feedback of routine characterization information to the materials growth effort, and (2) to develop new, innovative methods for materials characterization. Characterization
(Continues)

DD FORM 1 JAN 73 1473 EDITION OF 1 NOV 65 IS OBSOLETE
S/N 0102-014-6601

SECURITY CLASSIFICATION OF THIS PAGE (When Data Entered)

251 950

20. Abstract (Continued)

techniques described include routine Hall effect measurements, photoconductivity, contactless microwave magnetoconductivity, contactless infrared optical measurements, photoluminescence of bulk and interface states, and fabrication and test of Schottky barrier field effect transistors. Results achieved with these techniques on GaAs and InP materials produced in-house and provided by commercial laboratories are described.

CONTENTS

*On sabbatical leave from the U. of Ill., Chicago.

CHARACTERIZATION OF III-V MATERIALS

I. INTRODUCTION AND PROGRAM DESCRIPTION

Problems with availability, reproducibility, and reliability of GaAs and InP materials (particularly bulk, semi-insulating crystals) and microwave devices fabricated on these materials have been well-documented in various DoD sponsored programs over the past few years. This has led to a clear recognition of the need for thorough characterization of materials and processing effects as part of any materials growth/device development effort; it is anticipated that well-chosen characterization information should allow at least qualitative prediction of long-term device performance and reliability. The present materials characterization/device evaluation program is an integral part of a coordinated growth/characterization effort directed at the development and improvement of III-V compound semiconductors, in particular GaAs and InP, for microwave device applications. Since its inception, the overall objectives of the program have remained basically unchanged: (1) In the short term the goals are to provide rudimentary characterization information to the materials growth program on a rapid interactive basis which will identify needed areas of materials improvement; examples range from carrier type and mobility, obtained from Hall measurements, through more complicated measurements such as the identification of chemical impurities from helium temperature photoluminescence, to device fabrication and testing. (2) In the long term the objectives are to investigate and develop new innovative methods of characterization which, in

Note: Manuscript submitted January 13, 1978.

conjunction with existing techniques, will provide the necessary and sufficient information to predict reliable device performance. Implicit in this is the necessity for an in-depth understanding of what is being measured by the various techniques, and how these measurements are related to various material and device properties of interest. In many cases this in-depth understanding does not exist and must be acquired (a particularly important example is the detailed identification of deep level impurities and defects by various techniques and their role in bulk substrate material, as well as in the active layers, in limiting device performance.). Feedback from the characterization-device evaluation studies determine needed areas of material improvement as well as process related problems.

During the past year the characterization program has been predominantly carried out at the Naval Research Laboratory (NRL) and the Naval Ocean Systems Center (NOSC), with one task (scanning electron microscopy) at the Naval Surface Weapons Center (NSWC), White Oak. The latter work is included in the report of the companion Materials Growth program. Numerous techniques for characterizing material and device properties have been developed and utilized during the course of this program. Particular emphasis has been placed on contactless, non-destructive methods. These techniques include: (1) Contactless photoluminescence measurements to determine the presence of deep impurities (e.g. Fe, Cr, 0); shallow acceptor impurities (C, Si, Ge, Sn, Zn, Cd, etc.); and defect centers which may result during growth or processing, e.g. heat treatments; (2) IR reflectance and absorption for contactless measurement of average carrier density and mobility as well as the

determination of non-electrically active impurities from local mode spectra; (3) microwave magnetoconductivity for simple contactless measurements of mobility and carrier density (described in the last annual report); (4) an automated, temperature scanning van der Pauw apparatus for measurement of carrier density and mobility and their thermal activation energies; (5) a C-V profiling apparatus for the determination of depth profiles of carrier density in epi-layers; (6) various transient-capacitance methods for the measurement of deep impurity and defect levels in bulk and epitaxial samples as well as depth profiling of deep levels in Schottky barrier device structures; and (7) a capability for fabrication and dc and r-f evaluation of device parameters of Schottky barrier field effect transistors on both GaAs and InP with gate lengths as small as 1 μm.

During the past year, there has been continued emphasis on the characterization of semi-insulating GaAs particularly the NRL "undoped" material. A complete understanding of this material has not yet been achieved. In addition, efforts have expanded to include surface degradation of heat treated GaAs substrates, epitaxial GaAs, the interface between substrate and epitaxial layer, ion-implanted GaAs, and bulk InP.

All of these efforts have been closely tied to related 6.1 studies at NRL and NOSC. These studies are supported by NRL in-house 6.1 funds, NOSC IR funds and ONR 6.1 contract funds. In some cases the work is so closely intertwined that it is difficult to separate the 6.1 and 6.2 efforts which are mutually dependent; this is reflected to some degree in the remainder of the report, particularly sections II and III.

The main body of the report is divided into three major sections, II. Electrical Characterization, III. Optical Characterization, and IV. Device Fabrication and Evaluation (the device test structure is the Schottky Barrier Field Effect Transistor), which describe details of the work carried out during the past year. Section V summarizes the status of the program and presents recommendations for future work in areas that are incomplete or poorly understood.

II. ELECTRICAL CHARACTERIZATION

A. Introduction

During the past year the techniques for "electrical" characterization (the characterization of those parameters which determine the electrical characteristics of the material under investigation) have continued to evolve and one "new" technique, transient capacitance spectroscopy, has been developed and added to this program. Much of the effort in this area has been concerned with van der Pauw Hall effect measurements, which remains among the most useful of all analysis techniques. Standard Hall measurement at room temperature and liquid nitrogen temperature have been carried out on numerous bulk GaAs and InP samples as well as on epitaxial GaAs layers, and the resulting information on resistivity, carrier density, and mobility have been provided to the crystal growth program. In addition, a back-up manual Hall effect measurement system has been designed and is being assembled for use in the crystal growth area. Due to the importance of careful temperature dependent Hall measurements in the detailed characterization of the bulk semi-insulating GaAs and InP and the long times required for equilibrium in these samples, a completely automated temperature scanning system has been designed around a Tektroniks Graphics Display Computer. The system has been constructed and is undergoing final testing.

The contactless microwave magnetoconductivity technique for determining carrier mobilities described in last year's report has been used infrequently for routine epi-layer characterization. The efforts here have been largely directed at studies of annealing

behavior in ion-implanted GaAs, which has been largely supported outside the characterization program.

In the following sections a convenient graphical approach for evaluating Hall effect data in nearly intrinsic semi-insulating GaAs is described, and several approaches to transient capacitance spectroscopy for the evaluation of deep trap levels in semiconductors are outlined with specific application to GaAs.

B. Hall Effect in Nearly-Intrinsic GaAs

The recent growth at NRL of semi-insulating gallium-arsenide free of intentional doping makes it necessary to have a convenient method for determining the correct electron and hole concentrations and mobilities for the nearly-intrinsic condition. A graphical approach has been selected which is intended to provide the crystal grower with a convenient technique for evaluating Hall-effect data with a minimum of calculation.

A measurement of the Hall coefficient and resistivity at one value of magnetic field, as is typically done, is not sufficient to establish all the necessary parameters. Consequently, in analyzing such data it is necessary to assume a value for either the mobility ratio, $b \equiv \mu_n/\mu_p$, or the hole mobility, μ_p. It is not yet clear which of these two parameters is most nearly constant from sample to sample. We have chosen to assume the mobility ratio constant and plot the apparent electron concentration and the true electron mobility versus the true electron concentration for suitably chosen values of the apparent mobility and mobility ratio.

Two plots of this type are shown in Figs. 1 and 2. As an example of the use of these plots, consider a Hall measurement indicating n-type material with an apparent mobility of 1000 cm^2/volt-sec and an apparent carrier concentration of $5x10^6 cm^{-3}$. Fig. 1 is appropriate for these conditions and an assumed mobility ratio of 10. In analyzing the data one first draws on the plot a line at the indicated apparent electron concentration, $n_{app} = 5x10^6 cm^{-3}$. There are two intercepts with the curve which occur at true electron concentrations of approximately $6x10^5 cm^{-3}$ and $4.9x10^6 cm^{-3}$. The appropriate electron mobility is given in the lower half of Fig. 1 for the indicated concentrations. On multiplying the scaled mobilities by n_{app} and dividing by $1x10^6$ one gets 4200 cm^2/volt sec. and 1000 cm^2/volt sec., respectively. Thus, in this case, there are two possible, and acceptable solutions: $n \approx 6x10^5 cm^{-3}$, $\mu_n \approx 4200$ cm^2/volt sec. and $\mu \approx 4.9x10^6$, $\mu_n \approx 1000$. The choice must be made with the help of some other knowledge of the crystal growth conditions.

Frequently there is only one acceptable solution due to an extremely high ($>10^4 cm^2$/volt sec.) mobility associated with the low concentration solution. Such an example is shown in Fig. 2. This plot is drawn for a specific sample (4-25L) for which the Hall data gave $n_{app} = 8.1x10^8 cm^{-3}$, $\mu_{app} = 101$ cm^2/volt sec. The low concentration solution is $n \approx 1.8x10^5 cm^{-3}$, $\mu_n \approx 5x10^4 cm^2$/volt sec. Clearly, the required mobility is unreasonably high so the first solution must be rejected. As usual the second, and in this case the only acceptable, solution is essentially equal to the apparent

numbers. That is, $n \approx 1.8 \times 10^5 cm^{-3}$, $\mu_n \approx 101$ cm^2/volt sec. This sample is, therefore, highly impure with a very low carrier mobility. Two additional specific examples are given in Figs. 3 and 4 for samples II-35 and II-40.

An earlier plot for sample II-40 is shown in Fig. 5. This data was calculated with the conventional value of n_i,[1] the intrinsic carrier concentration at room temperature, which is $n_i = 1.1 \times 10^7 cm^{-3}$. This plot for a mobility ratio of 80 has no solution. Mobility ratios exceeding 80 are required for a solution. A mobility ratio of this size is difficult to explain satisfactorily since it requires a large difference in the electron and hole scattering cross sections. This difficulty led us to question the accepted value for n_i. Thus, we now believe that the correct value may be as small as n_i-1.7 to $2 \times 10^6 cm^{-3}$ in agreement with recent experiments[2,3] but not with some earlier estimates.[4] Figs. 1 through 4 are plotted with $n_i = 1.7 \times 10^6 cm^{-3}$.

References:

1. S. M. Sze, Physics of Semiconductor Devices (Wiley, New York 1969).
2. D. D. Sell and H. C. Casey, Jr., J. Appl. Phys. 45, 800 (1974).
3. D. C. Look, to be published.
4. D. C. Look, J. Phys. Chem. Solids 36, 1311 (1975).

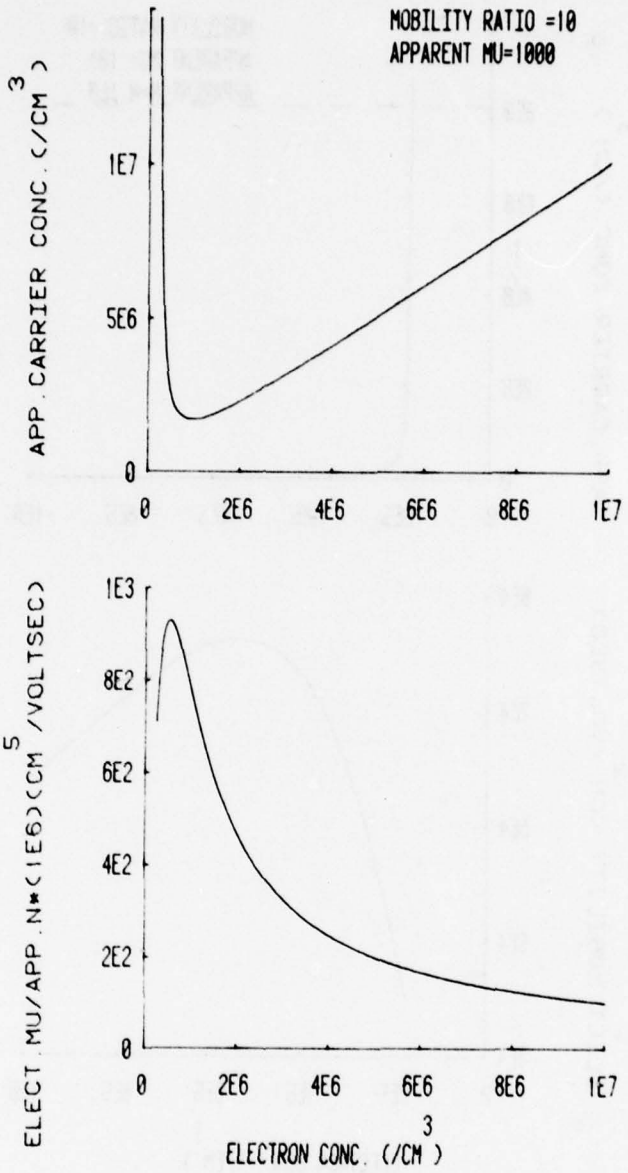

Fig. 1 — Apparent carrier concentration as determined by a Hall effect measurement (upper half) and true electron mobility (lower half) as a function of true electron concentration for GaAs. The electron-to-hole mobility ratio is taken to be 10. This plot is appropriate for a Hall measurement yielding an apparent electron mobility of 1000 cm^2/volt sec.

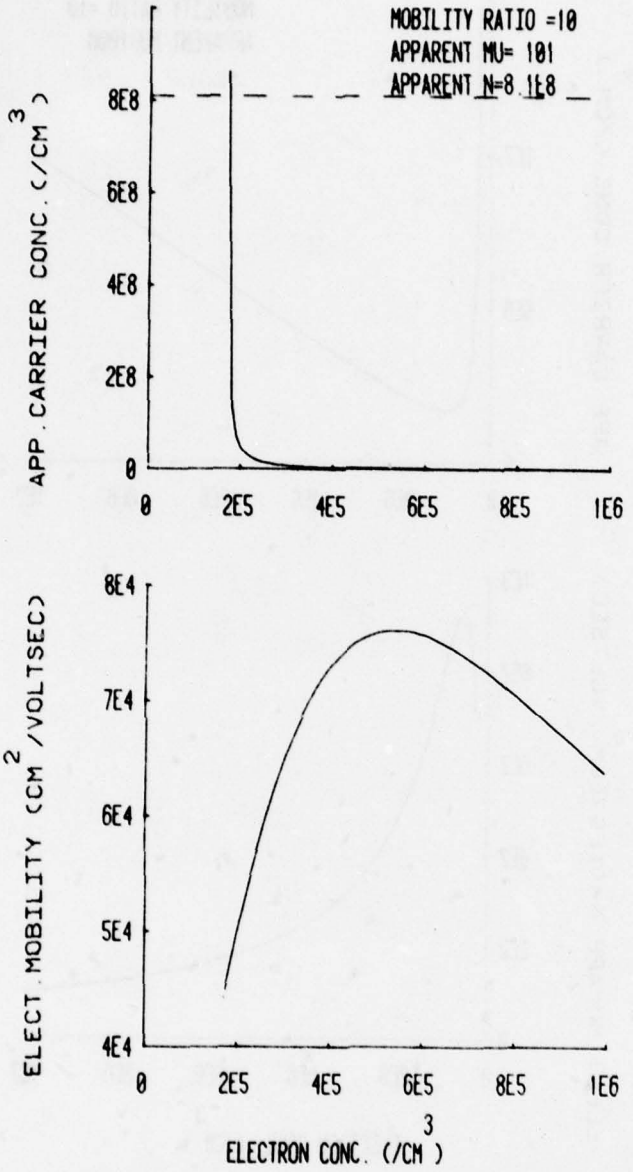

Fig. 2 — One of the two possible solutions for NRL sample 4-25L. This solution: $n = 1.8 \times 10^5 cm^{-3}$, $\mu_n = 5 \times 10^4 cm^2\ volt^{-1} sec^{-1}$ is rejected due to the unreasonably high electron mobility. The other possible solution is the apparent one: $\mu = 8.1 \times 10^8 cm^{-3}$, $\mu_n = 101\ cm^2 volt^{-1} sec^{-1}$.

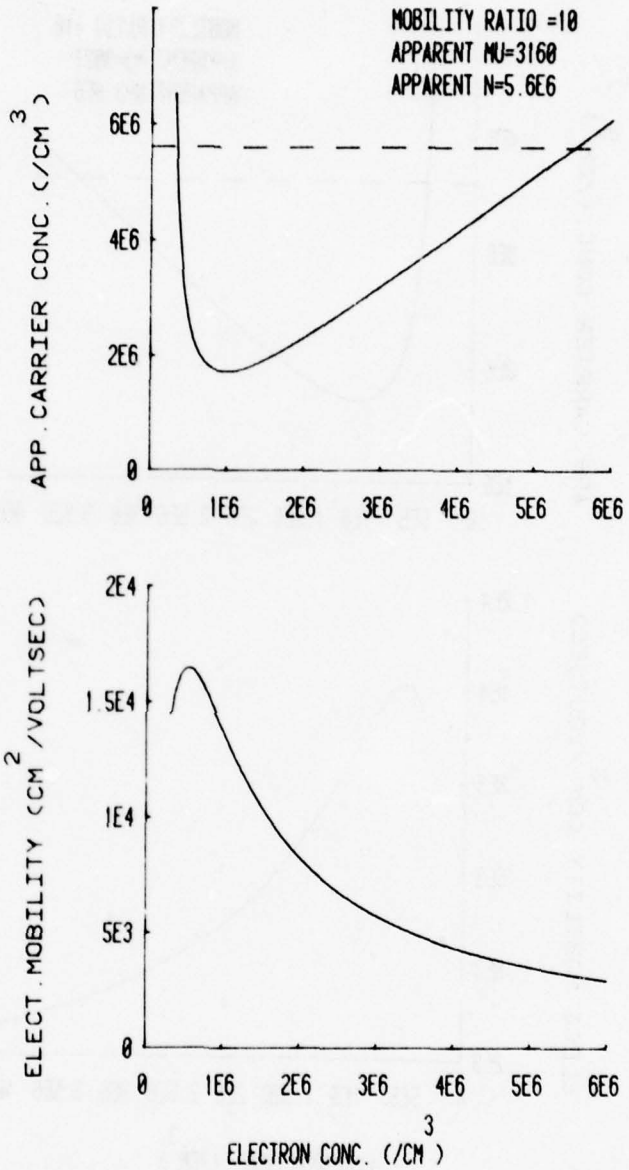

Fig. 3 — Two possible solutions for sample II-35. The low electron concentration solution requires a very high electron mobility.

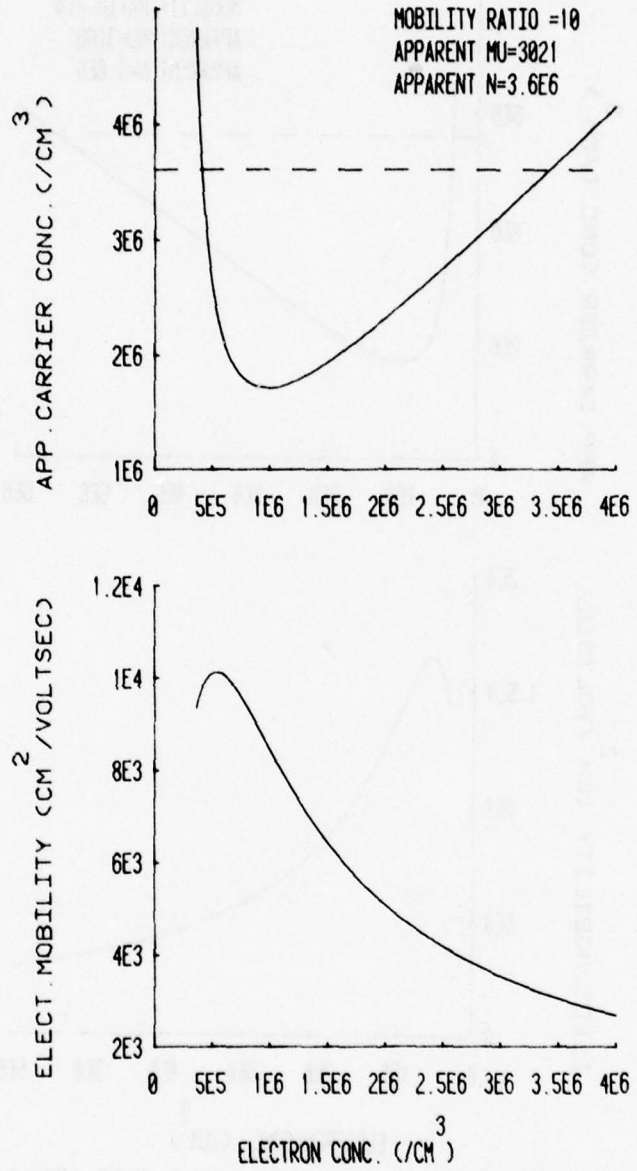

Fig. 4 — Two possible solutions for NRL sample II-40

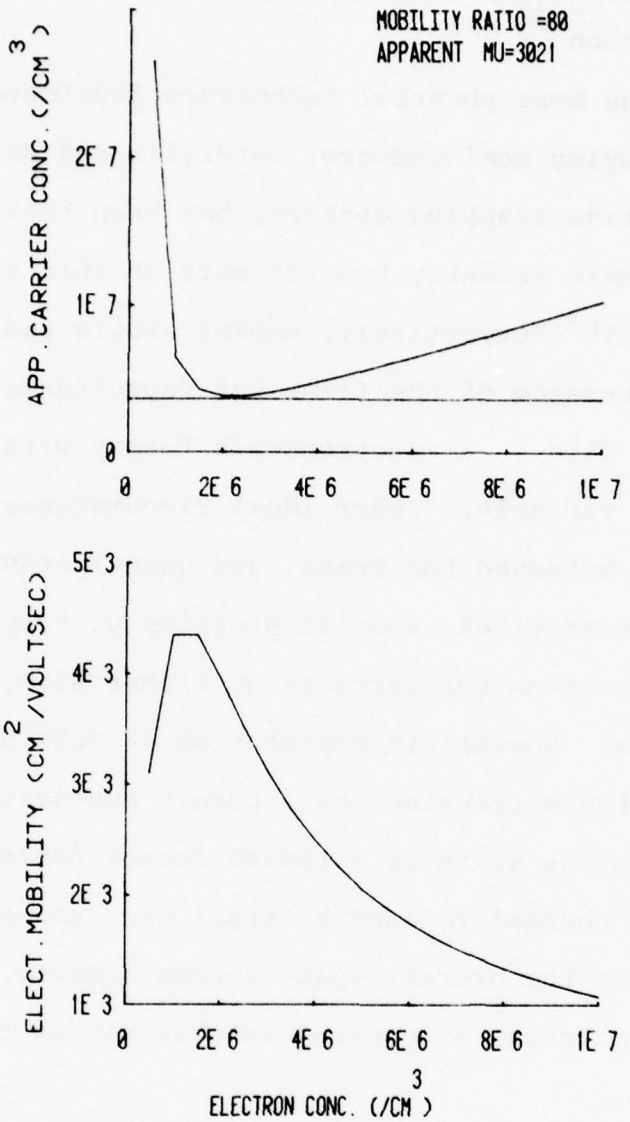

Fig. 5 — A plot for NRL sample II-40 for $n_i = 1.1 \times 10^7 cm^{-3}$.[1] A solution exists only for very high electron-to-hole mobility ratios. Recent results indicate that this value of n_i is in error.[2,3]

C. Transient Capacitance Spectroscopy

1. Introduction

One of the most powerful techniques developed during the last decade for surveying semiconductor materials and devices for their electrically active trapping centers, has been that of transient capacitance.[1] More recently two variants of this technique, known as DLTS[2] and DDLTS[3] respectively, employ single and double correlation analog processing of the transient capacitance waveform in order to obtain data in a spectroscopic format with temperature as the independent variable. Under ideal circumstances, samples may thus be readily surveyed for traps, and quantitative results obtained for: trap concentrations, spatial profiles of trap concentrations, capture cross sections for carriers of either sign, and carrier binding energies. Nominal interpretation of DLTS data requires that the capacitance transient be a purely exponential decay, as is the case when the width of a semiconductor depletion region responds to the thermal release by traps of a non-equlibrium charge small compared to the overall space charge density. Deviations from ideal exponential decay do present an obstacle to the interpretation of DLTS results.

In the experiments discussed here, MOS capacitors were fabricated on bulk n-type GaAs ($n\text{-}10^{15}/cm^3$ at 300K) using the anodization technique of Hartnagel.[4] This interface is known to have a high density of interface states, but the spatial discrimination of the DLTS and DDLTS techniques offers promise that bulk and surface effects may be separated. The use of a capacitor as the active element in these experiments limited the observations to majority carrier traps.

2. Analog Processing

Initial application of the DLTS technique to this system gave evidence of three strong majority carrier lines as shown in Fig. 6. From left to right, we will refer to these lines as L1, L2, and L3. The amplitude of L3 relative to L1 and L2 is underestimated by a factor of five in Fig. 6 because of the indicated change in gain. The upper and lower traces were obtained respectively from DDLTS and DLTS measurements on the same sample. In general, the capacitance transients from which these lines were obtained were not simple exponentials, and in each case the lines themselves were too broad, skewed to the low temperature side, and line amplitudes showed an anomalous dependence upon the rate window, an analog processing parameter.

In the DDLTS measurement the line L2 showed a reduction in width which could be due to a number of reasons. It may be that a significant portion of he single correlated, DLTS, signal originated in a portion of the depletion region which was not fully depleted of free carriers. Alternatively, the electric field in the depletion region is nonuniform, and a dispersion in carrier emission times can result if there is a strong electric field dependence in the capture cross section.

L3 is apparently resolved into two components when the double correlated, DDLTS, technique is employed. However, there is a special difficulty in that the very large amplitude of this line indicates either that this transient is not due simply to the release of trapped carriers, or if it is, then their concentration cannot be

assumed to be small compared to the overall charge density. Indeed, there is evidence that at least a portion of this strong line is associated with the formation of a surface inversion layer. The composition and amplitude of L3 was also found to be a complex function of reverse bias.

3. Digital Processing

Capacitance transients observed in these native-oxide capacitors deviated substantially from a purely exponential law. Using only DLTS studies varying rate window, reverse bias, pulse amplitude, and pulse width, it was not found possible to explain the DLTS spectra obtained. For this reason, additional evidence was obtained from digital analysis of the full capacitance transient at a number of temperatures. In each case the reverse bias and pulse amplitude were kept constant.

At least squares best fit of the observed transients was made to a five parameter model in which there were two exponential components, as indicated in EQ-1.

$$\Delta C = C_\infty + C_1 e^{-t/T_1} + C_2 e^{-t/T_2} \qquad (1)$$

The capacitance at infinite time, C_∞ , is poorly defined experimentally, so it was made the fifth adjustable parameter. The other four parameters are the amplitude and decay time of each of the two components. This model fit the observed decays well. For example, the maximum fractional deviation between the data and the fit was 0.2% for the transient shown in Fig. 7. Typically, the maximum fractional deviation was about 0.5%.

Fig. 8 summarizes the results of this digital decomposition of the observed capacitance transients at various temperatures. On the same plot is shown a summary by Mircea[5] of the trap release times which have to date been reported in GaAs. The fitting routine used also provided the 95% confidence limits for the decay time under the assumption that the five parameters are uncorrelated. Though there is, in fact, a correlation between some of the parameters, the 95% confidence limits still indicate the sensitivity of the fitting process to a variation of just one parameter. Therefore, these confidence limits are shown in Fig. 8 as error bars on each data point. Beside each point is also indicated the amplitude in picofarads of that decay component, as determined by the fitting routine. Reverse bias and pulse height were the same for all of the measurements so that the same region of the sample might be sampled.

The majority of the decay components shown in Fig. 8 are grouped near the emission times reported for two electron traps, EL-16 and EI-1 in the notation of Mircea.[5] These two levels were reported in different vapor phase epitaxial samples of GaAs. Within each grouping the measured decay amplitudes are nearly constant, with amplitudes of 1 and 2 pF for the points near EL-16 and EI-1 respectively. A much larger, 3.3pF, decay amplitude is measured at the point where the emission times of the centers EI-1 and EL-3 are equivalent. Attempts to resolve EL-3 at other temperatures using a seven parameter model have not yet been successful.

A total of three points on Fig. 8 seem unassociated with the centers mentioned above. Two of these appear to be unassociated also

with any of the emission times reported to date. The final component has a very large amplitude, 11 pF, and would appear to be associated with the center EB-3, a trap observed in electron irradiated GaAs. Data outside of the range of Fig. 8 reinforces this relationship to the center EB-3.

4. Discussion

At present many of the centers and mechanisms operating in these native-oxide capacitors are unknown, and it is not possible to calculate directly the observed analog line shapes given only the trap parameters as obtained from digital analysis of the capacitance transients. However, some assignments can be made. The excellent digital fits and the consistency in the decay amplitudes as provided by the fitting process, indicate the probable presence of the center EI-1, which would be a principal contributor to the line L2. It appears likely that the center EL-16 is present. Modeling of the DLTS line expected from this center using presently accepted parameters makes it appear unlikely that this component contributes to the line L2.

The very large amplitudes measured for both the line L3 and the decay component associated with EB-3, argue that this component is responsible for at least a part of the line L3. More significantly, it is known that this transient is not due to the release of carriers trapped at a center, but is due to the formation of a surface inversion layer. The large capacitance transient is observed to begin at a value of capacitance equal to the deep depletion capacitance at the bias point used, and to end at the value of capacitance as

determined by the presence of a mature surface inversion layer. At these low temperatures in GaAs minority carrier generation is accomplished by a two-step thermal excitation involving some trap near midgap. It is therefore expected that the time for inversion layer formation will show a variation with temperature characteristic of the slower of the two excitations. In this case, it would seem an electron emission from the center EB-3 is involved.

High interface state densities due presumably to disorder and non-stoichiometry are thought to be characteristic of these anodic oxides on GaAs. If this is true, it is not unreasonable that minority carrier generation times at the interface would be controlled by "disorder" traps, of which EB-3 is surely only one example.

References:

1. C. T. Sah, Sol. State Elect. 19, 975 (1976).
2. D. V. Lang, J. Appl. Phys. 45, 3023 (1974).
3. H. Lefevre, M. Schulz, Appl. Phys. 12, 45 (1977).
4. H. Hasegawa, K. E. Forward, and H. L. Hartnagel, Appl. Phys. Lett. 26, 567 (1975).
5. G. M. Martin, A. Mitonneau, and A. Mircea, Elect. Lett. 13, 191 (1977).

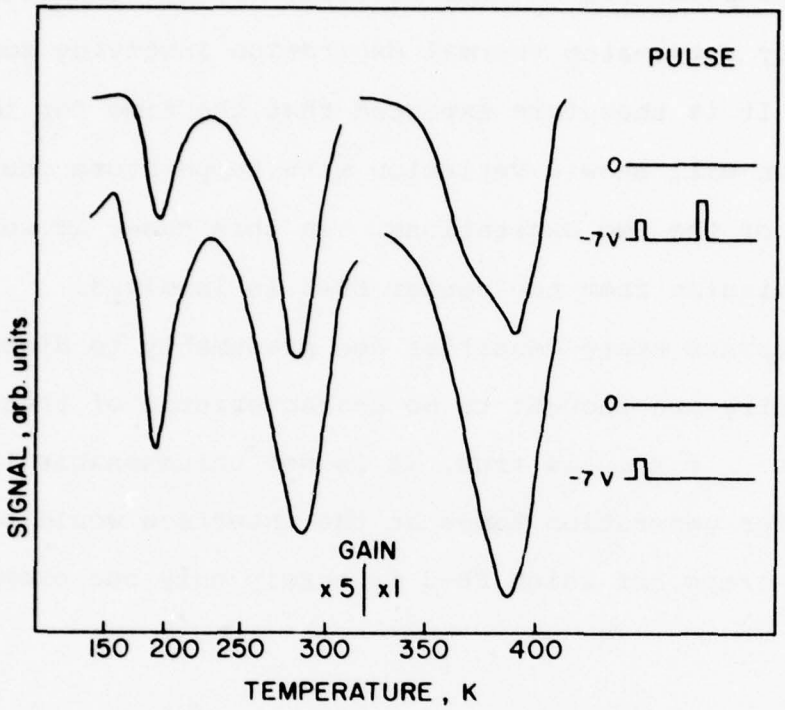

Fig. 6 — Singly correlated (DLTS) and doubly correlated (DDLTS) analog processing of the capacitance transients in the same native-oxide GaAs capacitor, produces the lower and upper spectra respectively. Both techniques limit to a certain energy window those traps which can contribute to the signal. Through the use of two different pulses for trap filling, the doubly correlated technique also provides a small spatial window.

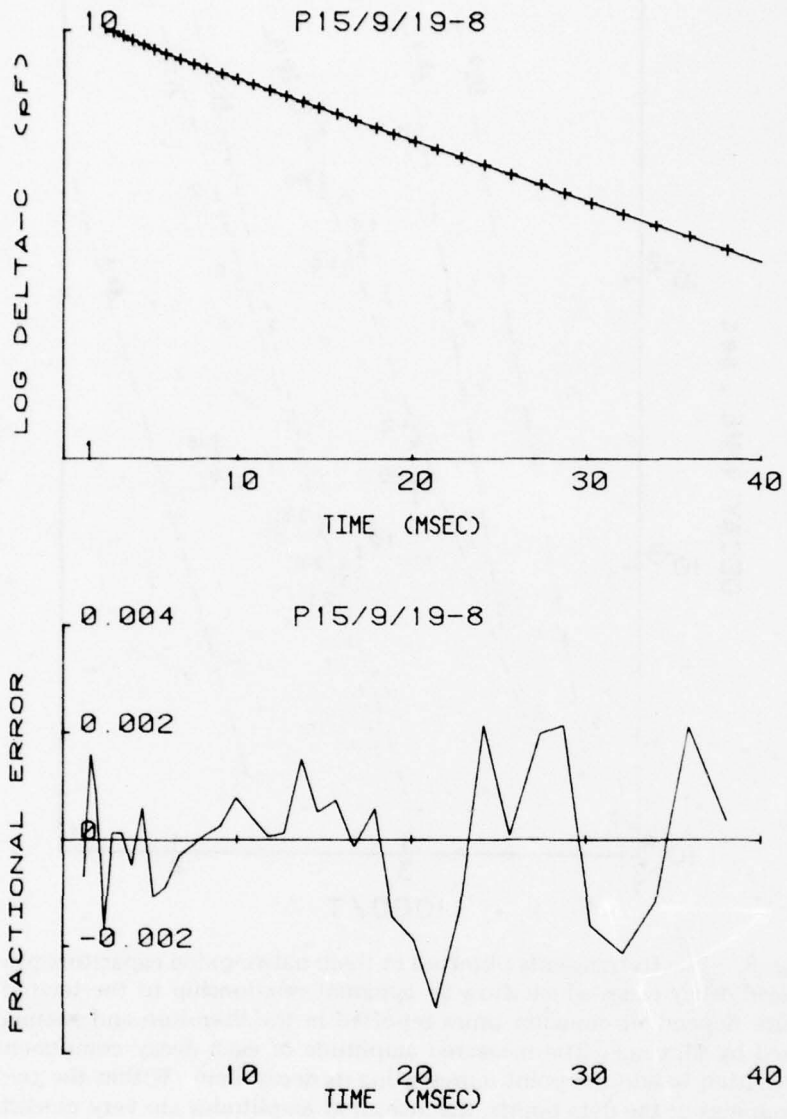

Fig. 7 — Capacitance transients were represented to a high degree of accuracy by a five parameter model assuming two purely exponential decay components. In this example the fractional error between the data and the fit was less than 0.2%. The decay times and amplitudes were: 1.8 ms with a 1.0pF amplitude and 30 ms with a 10.6pF amplitude.

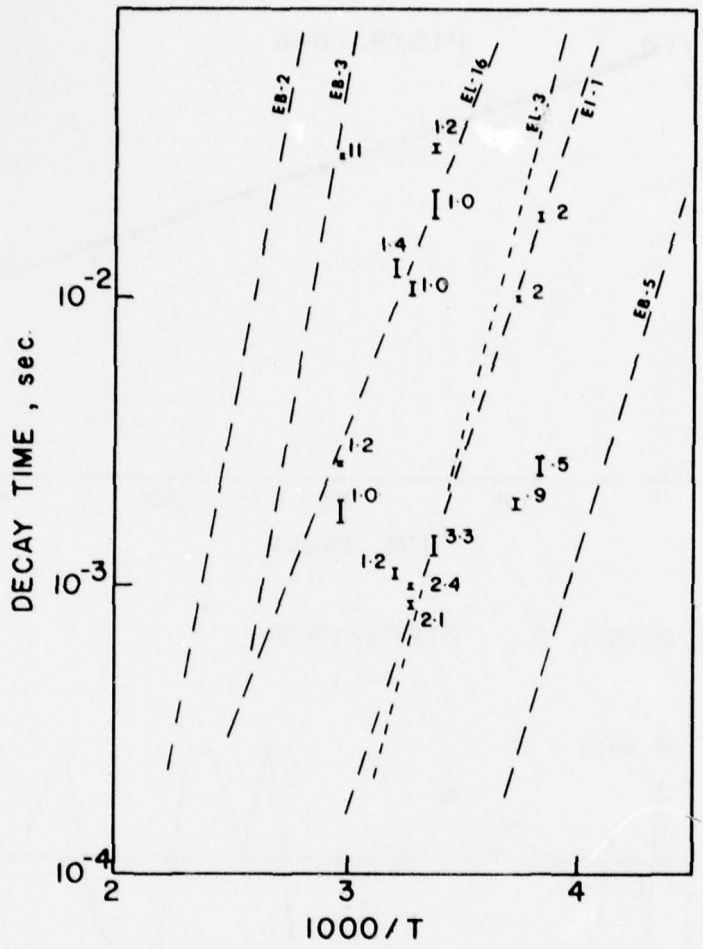

Fig. 8 — Fits to transients observed in these native-oxide capacitors produced decay times which show an apparent relationship to the temperature dependent emission times reported in the literature and summarized by Mircea.[5] The measured amplitude of each decay component is written beside the point representing its decay time. Within the two groupings of the data points, the measured amplitudes are very consistent. One very strong component, represented by the point in the upper left corner, is associated with the formation of a surface inversion layer.

III. OPTICAL CHARACTERIZATION

A. Introduction

During the past year, optical characterization studies have concentrated in two areas: (1) Photoluminescence measurements and (2) Infrared local vibrational mode spectroscopy.

Photoluminescence (PL) characterization studies of shallow and deep impurities in GaAs and InP have focussed on three major topics: (1) "type-converted" surface layers on various heat treated GaAs substrates, and the interface between these layers and liquid phase epitaxial (LPE) layers. This work was carried out jointly at NOSC and NRL with the NOSC work concentrating on the interface aspects via controlled doping of the epilayers and resulting modifications of the interface. (2) iron as a deep acceptor in InP, and (3) continuing work on Cr and other deep centers in GaAs. In addition, LPE layers of GaAs grown at NRL have been characterized by PL techniques and compared with epilayers from other sources; and a PL study of implanted Be shallow acceptor luminescence in GaAs was initiated. Finally, infrared (IR) local vibrational mode spectroscopy of NRL bulk "undoped" GaAs was initiated in the past year. These preliminary studies have revealed the presence of B on Ga sites in this material.

These efforts are described in detail in the following three sections.

B. PL Characterization of Bulk and Epitaxial GaAs and Bulk InP

1. Introduction

The acquisition of a Janis variable temperature optical cryostat has made it possible to study the temperature dependence of PL in the 2 to 50K temperature range. Examples of the application of this capability include a study of the temperature dependence of the 0.84 eV Cr zero phonon line in GaAs:Cr to clarify the recombination mechanism (following section), a study of the temperature dependence of the sharp zero-phonon spectra in InP:Fe (section III.B.3), and the resolution of free to bound and donor-acceptor radiative recombination transitions in the near band-edge PL spectra of GaAs (this is necessary for accurate chemical identification of the acceptor impurities).

In addition, PL has been used to examine thin ($\sim$ 3000 Å) Sn-doped active epitaxial layers grown on Ga-etched substrates to identify the residual impurities and to estimate the quality of the active layers and the interface. This work is also described in the following section.

2. Gallium Arsenide

Bulk GaAs:Cr

Our previous studies of GaAs:Cr identified a characteristic low temperature PL band with a sharp zero-phonon line at 0.838 eV and associated phonon structure at lower energies; this band was originally assigned to an internal excited state to ground state transition ($^5E \rightarrow {}^5T_2$) of Cr^{2+} (ionized acceptor) in tetrahedral symmetry in the usual crystal field notation (see

Fig. 9). An additional weak band with a peak near 0.56 eV and no resolved structure was observed and found to be correlated with the presence of Cr from a comparison of PL excitation and quenching spectra with optical quenching and enhancement ESR spectra. This was originally attributed to a band to center recombination transition involving Cr^{3+} (charge transfer transition). Other workers[2] have also observed the band near 0.8 eV, but have attributed the recombination process to a radiative transition from the conduction band to the ground state of Cr^{2+}. It is important to clarify the nature of the recombination in GaAs:Cr in order to determine accurately the ground state energies of the various Cr charge states so that a microscopic picture of the compensation process can be developed, and Hall measurements on semi-insulating material can be analyzed in detail.

In order to clarify this situation we have carried out a series of higher resolution, temperature dependent studies of the PL bands associated with Cr in both bulk and epitaxial GaAs, the latter in collaboration with H. Stocker (presently of Bell Labs, Murray Hill). Fig. 10 shows high resolution spectra in the 0.56 and 0.80 eV spectral regions in a bulk sample of GaAs:Cr obtained from Siemens. The 0.56 eV band has been resolved into a zero phonon line (or lines) and vibrational mode structure for the first time. This observation, the temperature dependence studies discussed in the following paragraphs, and the detailed ESR studies carried out under ONR and internal NRL sponsorship in NRL Code 6450 have led us to propose the model of Fig. 11 for

the recombination transitions which are responsible for the 0.56 eV and 0.84 eV PL bands. The ESR measurements[3] have determined that the symmetry of Cr^{2+} is lowered from tetrahedral (T_d) to tetragonal (D_{2d}) via a strong Jahn-Teller effect which substantially splits the ground state ($^5T_2$) into a lower $^5B_2$ and an upper ^5E state; a similar but much smaller splitting takes place in the tetrahedral ^5E excited state. We suggest that both the 0.56 eV and 0.84 eV bands are due to intracenter transitions of Cr^{2+}; the zero phonon line(s) near 0.575 eV is due to a transition from either $^5B_1$ or $^5A_1$ to the upper ^5E state, and the 0.84 eV zero phonon line results from a transition from $^5A_1$ to the lower $^5B_2$ ground state. This implies a Jahn-Teller splitting of the ground state of the order of 0.27 eV, which is large but consistent with estimates from the ESR measurements.

The interpretation of the 0.84 eV band as due to intracenter transitions (rather than band to center) is consistent with detailed measurements of the temperature dependence of the line width of the zero phonon line. For a band to acceptor radiative recombination transition the lineshape is expected to depend on the temperature according to a simple convolution of the density of states with the Boltzmann factor, provided the matrix element for the transition is not strongly dependent on energy over the range of energies determined by the temperature variation.[4] Thus, the PL intensity is given by

$$I \propto E^{\frac{1}{2}} \exp(-E/kT) \qquad (1)$$

where E is the energy measured relative to the difference between the band edge and the ground state of the center.

Results at two temperatures along with calculated lineshapes are shown in Fig. 12. Several aspects of the data are noteworthy. At the higher experimental temperature a reasonable fit is obtained only for an assumed temperature significantly lower than that measured. On the other hand, at the lower experimental temperature a much higher temperature in the calculated lineshape is required to obtain a reasonable fit to the data. Also note that a shoulder appears on the high energy site of the experimental line; this was reproducible and indicates that the zero phonon line is composed of at least two lines.

The temperature dependence of the experimental linewidths for three samples and the predictions of the Eagle's formula (Eq. (1)) are summarized in Fig. 13. The experimental data deviate by nearly a factor of 2 at "high" and "low" temperatures from the calculated linewidths; the experimental linewidths are <u>larger</u> at low temperatures and <u>smaller</u> at high temperatures.

We conclude that band to center recombination cannot explain the experimental observations, and the recombination is most likely via intracenter transitions as discussed above, perhaps with the excited state degenerate with the conduction band continuum. This means that the PL energy for this transition is <u>not</u> simply the difference between the ground state of the Cr^{2+} center and the conduction band edge, and additional measurements are required to determine this energy accurately.

LPE GaAs:Sn

Photoluminescence measurements have been carried out on a number of NRL Code 5220 active LPE layers grown on semi-insulating substrates in a preliminary attempt to determine if photoluminescence can be used to characterize such layers for microwave FET applications. The epi layers investigated were n-type, Sn-doped single crystals with carrier concentrations in the $10^{17}cm^{-3}$ region grown on semi-insulating substrates.

A Ga etch-back was used to remove the "type-converted" layer which results from the pregrowth heat treatment of the substrate (see section III.C.). Results at 4.2K over a fairly broad spectral range are shown in Fig. 14 for three samples which were grown under similar conditions from Sn-doped melts. Rather substantial differences in the PL spectra are observed. A systematic variation on the energy position of donor-acceptor pair recombination line apparently associated with carbon acceptors is observed from low net electron density (II-74N) to higher densities (II-82N). It should also be noted that the position of these lines is a rather strong function of pump laser intensity. In II-74N a bound exciton line associated with Sn acceptors is observed at 1.506 eV. This line moves to higher energies as the net donor concentration increases. The bound exciton line at 1.514 eV in II-74N also moves up in energy as the net donor concentration increases. At much lower energies a weak band associated with Sn acting as an acceptor is observed in all samples near 1.36 eV. This band is shown more clearly at higher sensitivity in Fig. 15 for each of the samples. It is not certain if this band is associated with a simple acceptr (Sn substituting for

As) or is due to a more complex acceptor center associated with Sn. Nevertheless, it is clear that a measurable amount of the Sn used to dope the active layer n-type produces undesirable compensating acceptor centers. Additional careful work is required to make PL a useful routine characterization tool for the active epitaxial layers, and to relate these measurements to characteristics of microwave FETs fabricated on similar active layers. Such measurements are currently underway.

References:

1. W. H. Koschel, S. G. Bishop, and B. D. McCombe, Solid State Commun. 19, 521 (1976).
2. H. J. Stocker and M. Schmidt, Proc. of the XIIIth Int'l Conf. on the Physics of Semiconductors, ed. F. G. Fumi (Tipografia Marves, Rome, 1977), p. 611.
3. J. J. Krebs and G. Stauss, Phys. Rev. B16, 971 (1977).
4. D. M. Eagles, J. Phys. Chem. Solids 16, 76 (1960).

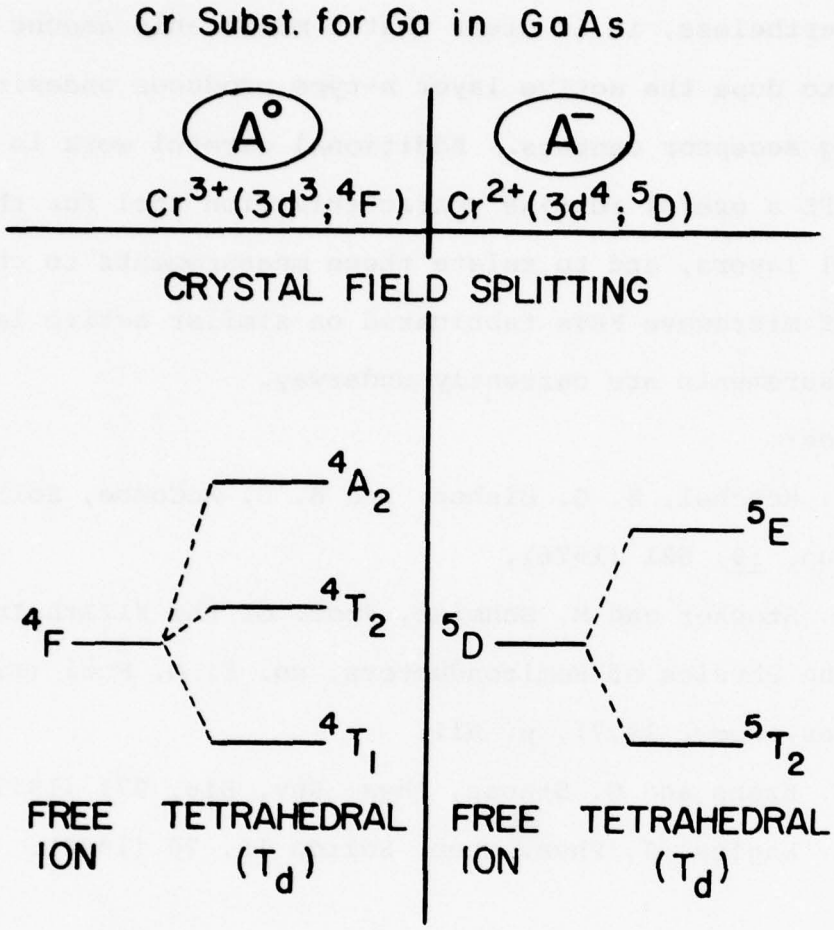

Fig. 9 — Schematic diagram of the energy levels of Cr^{2+} and Cr^{3+} for the free ions and for the ions in tetrahedral symmetry

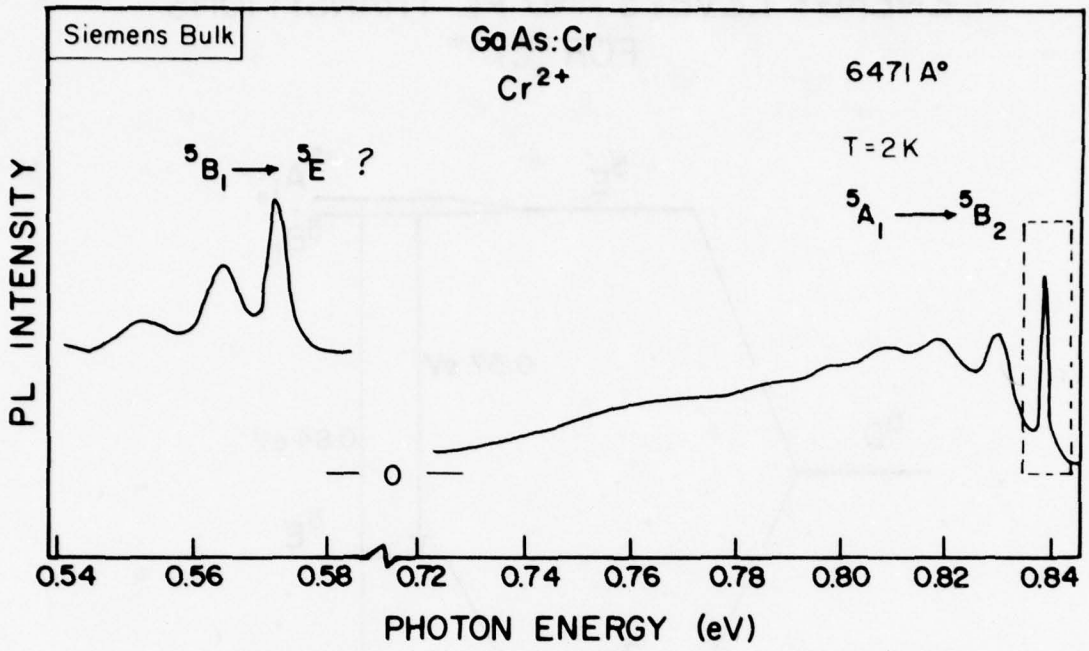

Fig. 10 — "Deep" PL spectrum of Siemens bulk GaAs; Cr showing the two separate bands in detail. The possible transitions of Cr^{2+} responsible for the 2 bands are indicated.

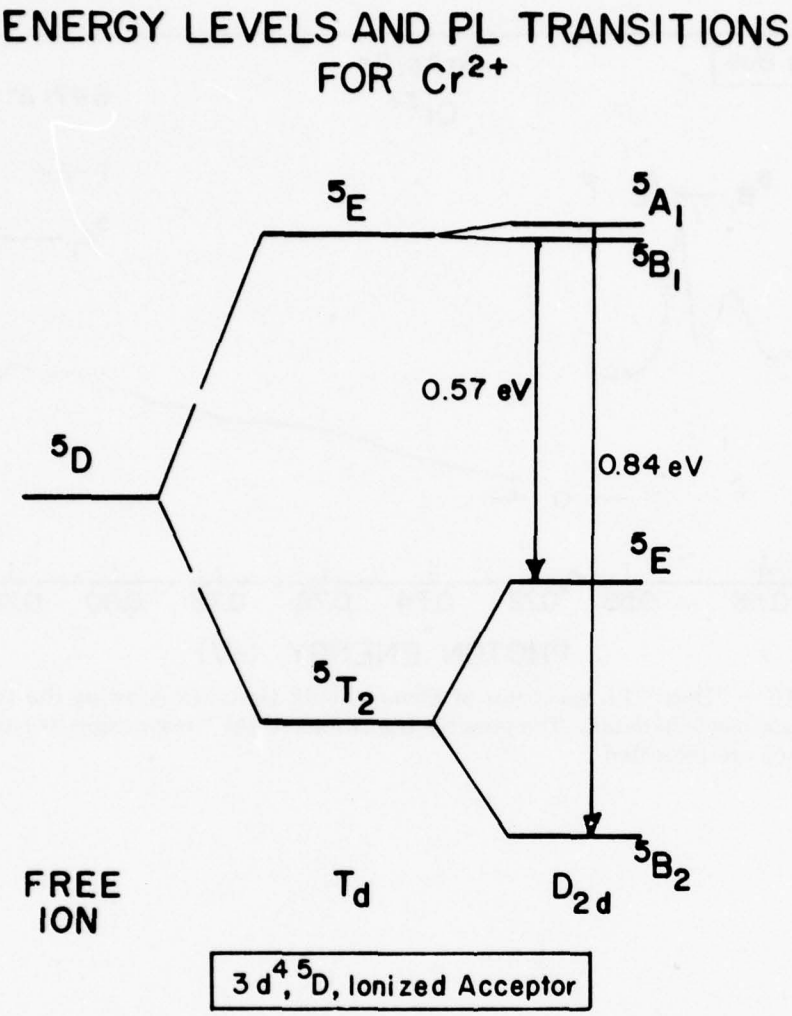

Fig. 11 — Schematic energy level diagram for Cr^{2+} in various symmetry environments. The possible transitions which could account for the PL spectra of Fig. 10 in the Jahn-Teller distorted site (D_{2d}) are indicated.

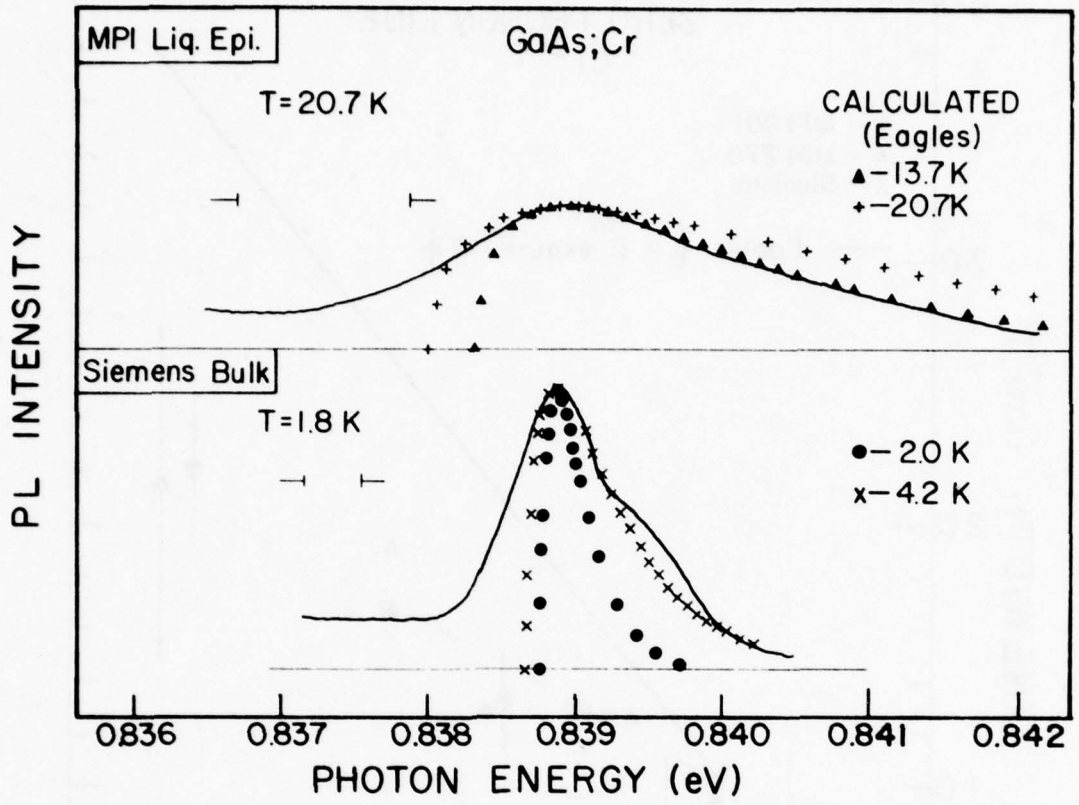

Fig. 12 — Experimental (solid lines) and calculated zero phonon lines for the 0.84 eV Cr PL. Temperatures are indicated.

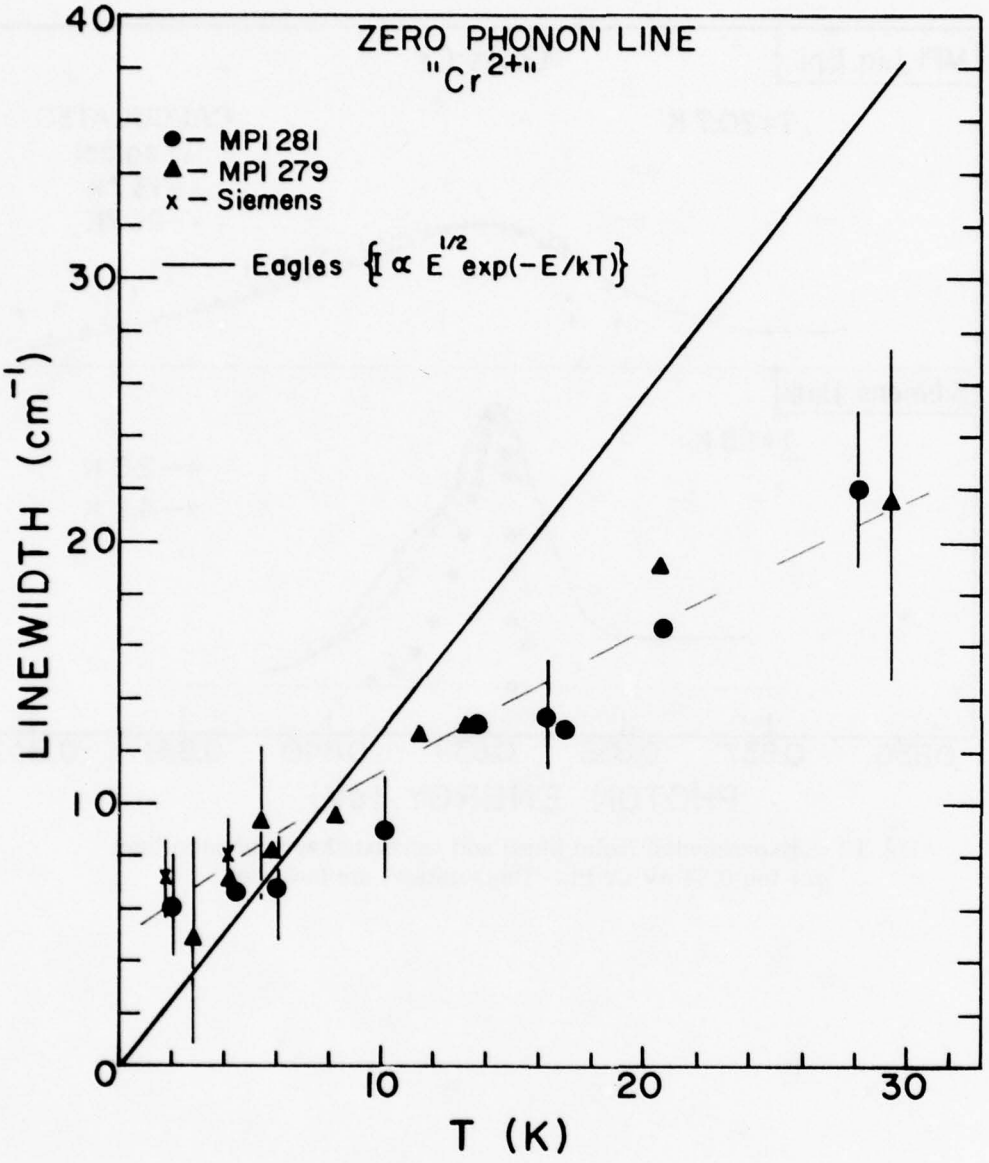

Fig. 13 — Experimental (symbols) and calculated (solid line) temperature dependence of the zero phonon linewidth for the 0.84 eV PL

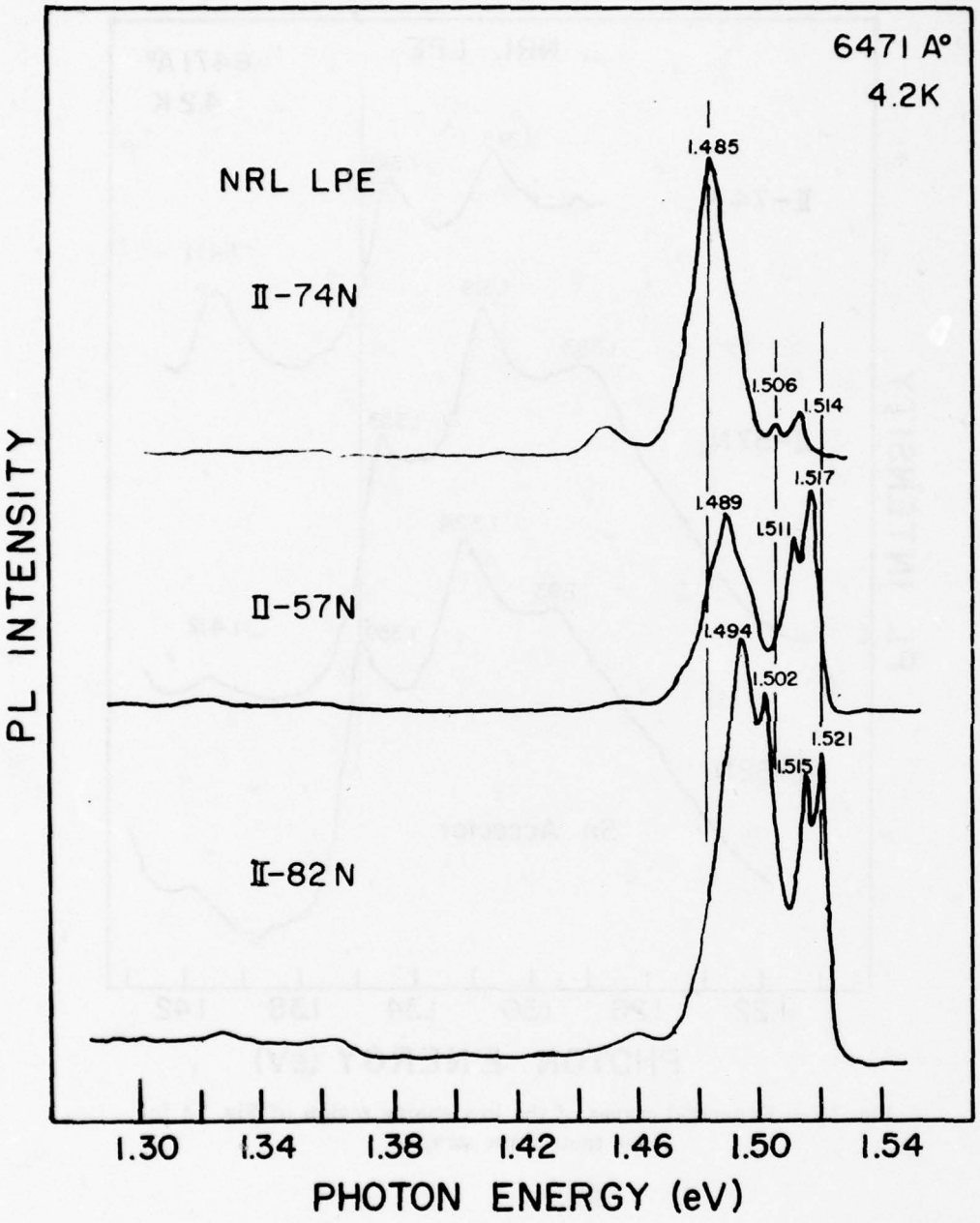

Fig. 14 — PL spectra of three NRL Sn-doped liquid epitaxial GaAs-layers. The photon energies of various features are indicated.

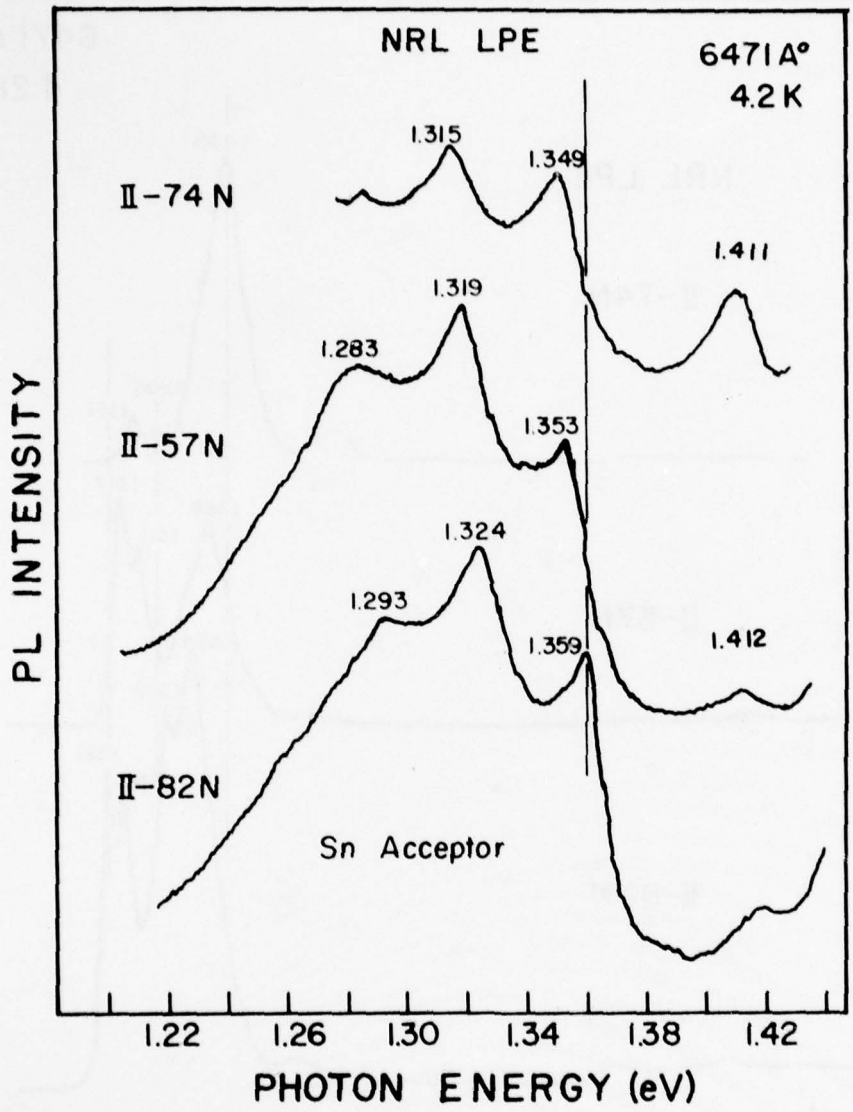

Fig. 15 — Expanded curves of the low energy region of Fig. 14 for the same three samples

3. InP:Fe

Iron doped InP exhibits a PL band at 0.35 eV with four well resolved zero phonon lines which have been attributed to transitions between the $^5T_2$ and ^5E crystal field levels of Fe^{2+} (ionized acceptor) in tetrahedral coordination (FIg. 16). The relative intensities of these lines have been observed to vary as a function of local strains in the sample, and for a highly strained sample, a fifth line appears above the dominant PL transition at $\sim$ 2830 cm^{-1} (Fig. 16).

The intensity of the 0.35 eV PL in InP:Fe has been studied as a function of Fe doping level for bulk samples with Fe concentrations ranging from unintentionally doped ($\sim 10^{15}$) to $\sim 2x10^{17}cm^{-3}$. In the most highly doped sample (1-44-H, N_{Fe} $\sim 2x10^{17}cm^{-3}$, the Fe PL at 0.35 eV is the dominant radiative recombination mechanism and no band edge luminescence is observed outside the noise. In a less heavily doped sample (1-91-H, N_{Fe} $\sim 10^{16}cm^{-3}$, ρ 10^7 Ω-cm) the Fe Pl at 0.35 eV is again the dominant radiative recombination; in fact this band is roughly a factor of 5 more intense than the 0.35 eV band in 1-44-H for the same pump laser intensity. For 1-91H, however, substantial band edged luminescence is observed; this includes an exciton band and recombination via neutral acceptors, which in this case appear to be Zn. In addition, a broad band luminescence peaked at $\sim$ 0.5 eV is observed in this sample. In the unintentionally doped InP (1-81-H, n-type, n $\sim 4x10^{15}cm^{-3}$) the band edge emission is the dominant radiative recombination mechanism although a weak Fe PL spectrum can still

be observed at 0.35 eV indicating that trace amounts of Fe are introduced as a contaminant in the bulk material during the crystal growth process.

These studies indicate that Fe is an efficient radiative recombination center in InP. It also appears that the broad 0.5 eV band is correlated with the presence of Fe, but the recombination process is not clear as yet.

The PL excitation (PLE) spectrum for the 0.35 eV Fe luminescence is 1-44-H is shown in Fig. 11. The excitation spectrum has one peak 1.42 eV associated with the fundamental band edge absorption and a weaker, broader peak at about 1.3 eV associated with an unidentified extrinsic absorption. This same 1.3 eV peak is observed in the excitation spectrum for optical enhancement of the strong Fe^{3+} electron spin resonance signal in InP:Fe. This, in part, has led to the suggestion that the radiative recombination process which involves the Fe center requires the presence of Fe^{3+} ions in the equilibrium state. Upon optical excitation of electron-hole pairs an excited electron is captured by an Fe^{3+} forming an excited state of an Fe^{2+}. The excited state of the Fe^{2+} decays to the ground state by emission of a $\sim$0.35 eV photon. At present, this recombination scheme remains as an unsubstantiated hypothesis.

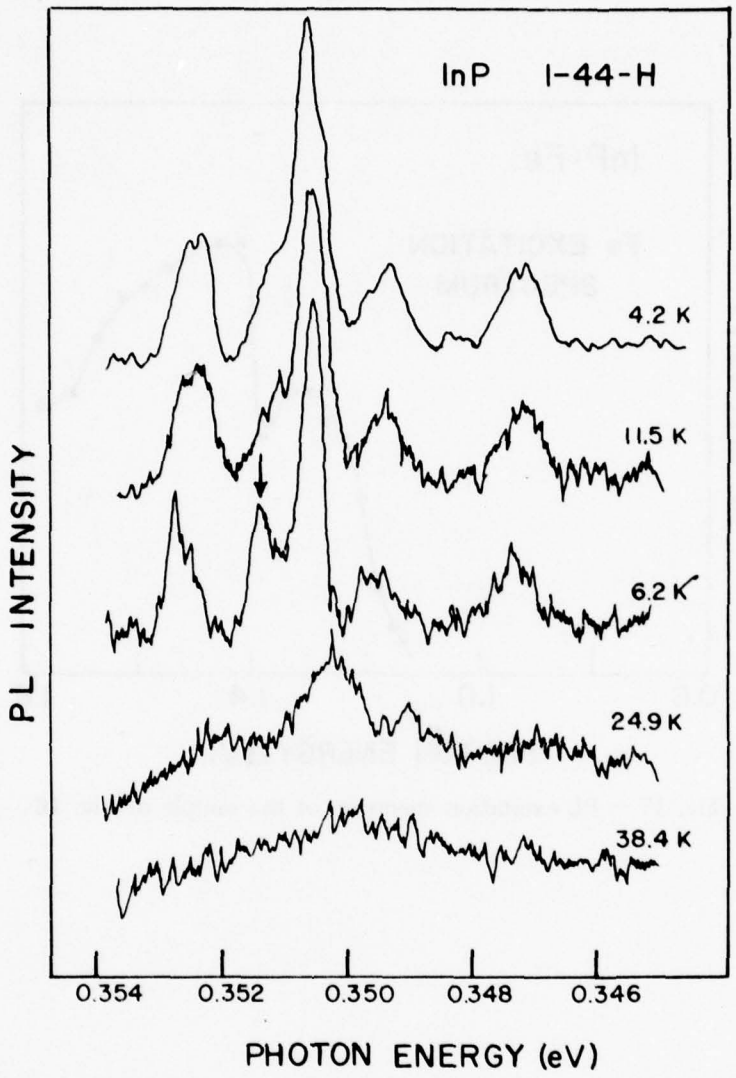

Fig. 16 — Fe^{2+} PL spectra for sample 1-44-H at several different temperatures. Only the sharp zero phonon multiples is shown. The fifth line which seen most clearly at temperatures slightly above 4.2K is indicated by the arrow.

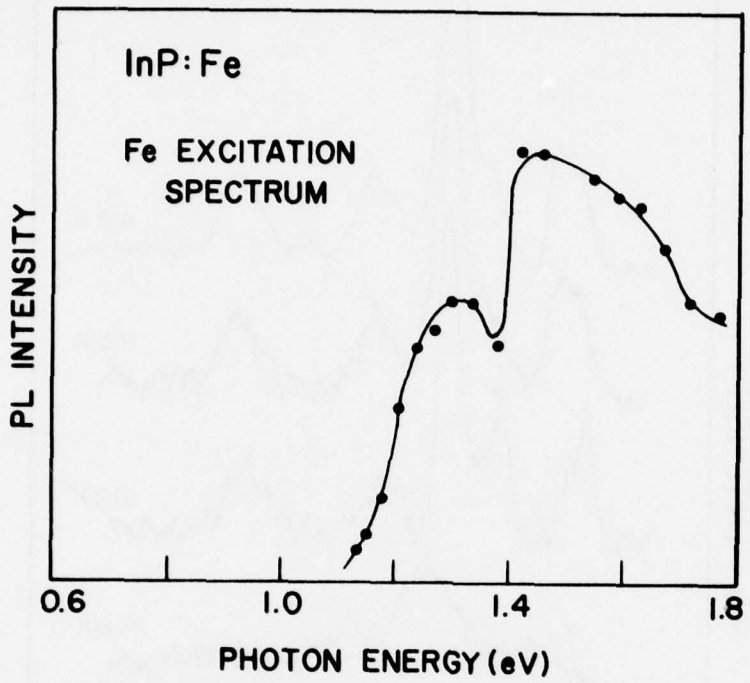

Fig. 17 — PL excitation spectrum of the sample of Fig. 16

C. Surface Degradation and Epitaxial Layer-Substrate Interfaces-GaAs

1. Introduction

Through joint experiments carried out at NRL and NOSC, we have established that the conducting layer (usually p-type) which forms on the surface of a semi-insulating GaAs substrate subjected to a typical LPE pre-growth heat treatment (740^{o}C for 30-100 min) is related to the formation of defects which can be detected and characterized by PL techniques.[1] A typical PL spectrum for NRL undoped semi-insulating GaAs is shown in Fig. 18; the spectrum includes a strong carbon shallow acceptor PL band (free to bound) at 1.494 eV and an additional "defect" related band at 1.413 eV. We have suggested that the latter band is attributable to a carbon acceptor-arsenic vacancy complex. Other workers[2,3] have obtained similar results and have proposed that the 1.413 eV band is due to Mn acceptors on Ga sites which must diffuse to the surface out of the bulk or diffuse into the surface layer from some external source. This assignment was made largely on the basis of a comparison with previous PL studies of Mn-doped MBE GaAs and Mn-doped LPE GaAs.

Further studies of this problem are presented in the following sections. These include investigations of heat treated bulk material, Mn-doped MBE epitaxial layers, and doped LPE layers grown on heat treated substrates. Although these studies are consistent with the suggestion that the PL band at 1.413 eV is due to an As-vacancy-acceptor complex, the possibility that it is related to Mn cannot be ruled out, particularly in view of the comparative

studies of heat treated material and Mn-doped MBE material discussed in the next section.

References:

1. W. H. Koschel, S. G. Bishop, B. D. McCombe, W. Y. Lum and H. H. Wieder, Proc. of the Sixth Int'l Conf. on GaAs and Related Compounds, Edinburgh, 1946, Conference Series #33a (The Inst. of Physics, London, 1977), p. 98.
2. J. Hallais, A. Mircea-Roussel, J. P. Farges, and G. Poibland, Proc. of the Sixth Int'l Conf. on GaAs and Related Compounds, St. Louis, 1976, Conference Series #33b (The Inst. of Physics, London, 1977), p. 220.
3. R. Zucca, Ibid., p. 228.
4. M. Ilegems and R. Dingle, Proc. of the Fifth Int'l Conf. on GaAs and Related Compounds, Deauville, 1974, Conference Series #24 (The Inst. of Physics, London, 1975), p. 1.
5. W. Schairer and M. Schmidt, Phys. Rev. B10, 2501 (1974).

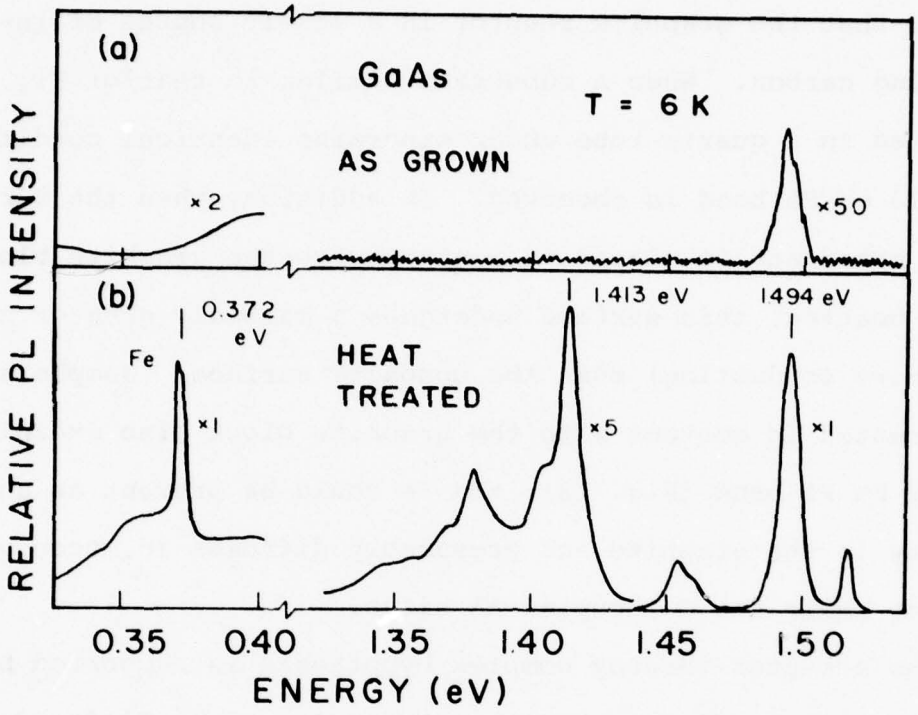

Fig. 18 — PL spectra of NRL undoped semi-insulating GaAs as grown and after a 100 min. heat treatment at 740°C in the LPE reactor

2. PL Studies of Surface Degradation on Bulk GaAs during the LPE Growth Cycle

Further studies of heat treated substrates have demonstrated that the graphite reactor is a likely source of in-diffusing carbon. When a substrate similar to that of Fig. 18 is heated in a quartz tube under otherwise identical conditions no 1.413 eV PL band is observed. In addition, when the surface of the substrate is placed in contact with the graphite block during heating, this surface undergoes a markedly greater conversion (more conducting) than the opposite surface. Sample surfaces heat treated in contact with the graphite block also exhibit a 0.37 eV Fe PL band (Fig. 18); the Fe could be present as an impurity in the graphite and presumably diffuses in, occupying Ga sites while the C occupies As sites.

The acceptor-vacancy complex hypothesis is supported by subsequent PL studies on heat-treated bulk n-type Si-doped GaAs carried out at NOSC and NRL. The surface of this material also exhibited evidence of the "defect" band but in this case the PL spectrum contains a Si shallow acceptor band at 1.487 eV, and the defect band is shifted to 1.409 eV (Fig. 19). We suggest that amphoteric Si atoms originally on Ga sites and acting as donors shift to As sites and become acceptors as As vacancies diffuse in from the surface during heating. Furthermore, the acceptor-vacancy complex now involves Si acceptors instead of carbon and as a result is shifted slightly to lower energies.

In order to test the Mn-hypothesis mentioned in the introduction, we have carried out a comparative PL study of the bands in

several of our heat treated GaAs samples and those in the Mn doped MBE GaAs samples studied by Dingle who has graciously made the samples available to us. The defect band from two heat treated NRL grown semi-insulating GaAs samples doped with Cr and Te ($N_{Cr} > N_{Te}$) as well as the bulk Si-doped GaAs described above are shown for comparison with the Mn-doped sample in Fig. 20. These samples were chosen because their main peaks occurred within 2 meV of 1.407 eV, the position in the Mn-doped sample. In other heat treated samples, including NRL undoped material, Laser Diodes material, and Crystal Specialties material the dominant peak was 4-6 meV higher in energy. Two additional Mn-doped MBE samples also showed similar bands with dominant peak at 1.411 eV. It must be concluded that the origin of this band in those samples is most likely the same, but the energy positions are a function of a number of other parameters; these include the chemical nature and density of shallow dopants and to a smaller degree the pump laser intensity. It should be noted that the heavily Cr and Te doped (both in the $10^{16}cm^{-3}$range sample (III-162) does not type-convert when heat treated, and the defect PL band is very weak and broad. The more lightly Cr and Te doped (in the $10^{15}cm^{-3}$ range) sample (III-28L) converted weakly p-type.

There are two possible explanations for the non-converting behavior of III-16L:1) simple compensation of shallow acceptors (the defects) by shallow donors (T_c); 2) competition for As sites by the Te during the thermal degradation. Process 2) would be equally effective for either the Mn acceptor or the acceptor-vacancy

complex; however, in order to compensate the typical p-type density observed ($10^{17}cm^{-3}$) in the type-converted layer, large amounts of Te would have to diffuse out of the bulk to the surface region. Process 2) would be doubly effective in preventing type-conversion if the acceptor-As vacancy complex model is correct since it reduces the number of As vacancies as well as compensating the defect acceptors. At present, it is not possible to differentiate between these possibilities.

PL studies of the type-converted surfaces in conjunction with successive anodic oxidation and stripping procedures determined that the converted layers are $\sim$ 2000-4000 Å thick. There is obviously a gradient in the concentration of the As vacancies and the diffused shallow acceptor species across this thin layer, and this manifests an effect upon the PL spectra analagous to results which we have observed in ion-implanted layers of shallow acceptors in GaAs.[2] The energy position of the shallow acceptor PL band shifts in energy as a function of the intensity of the exciting light. This shift is attributable to a power dependent profiling effect in which low power PL spectra are produced by recombination centers near the surface of the sample, while with increasing exciting light intensity the photo-injected carrier distribution probes recombination centers deeper in the sample. The low intensity excitation produces a PL spectrum whose energy position is characterized by the relatively high concentration of diffusing acceptors near the surface; the higher intensity spectrum includes radiation emitted at a slightly different energy by the acceptors in the lower concentration region lying deeper in the sample.

References:

1. M. Ilegems and R. Dingle, Proc. of the Fifth Int'l Conf. on GaAs and Related Compounds, Deauville, 1974, Conference Series #24 (The Inst. of Physics, London, 1975), p. 1.

2. S. G. Bishop, J. Comas, S. Sundaram, and B. D. McCombe, Appl. Phys. Lett., 15 Dec 1977, in press.

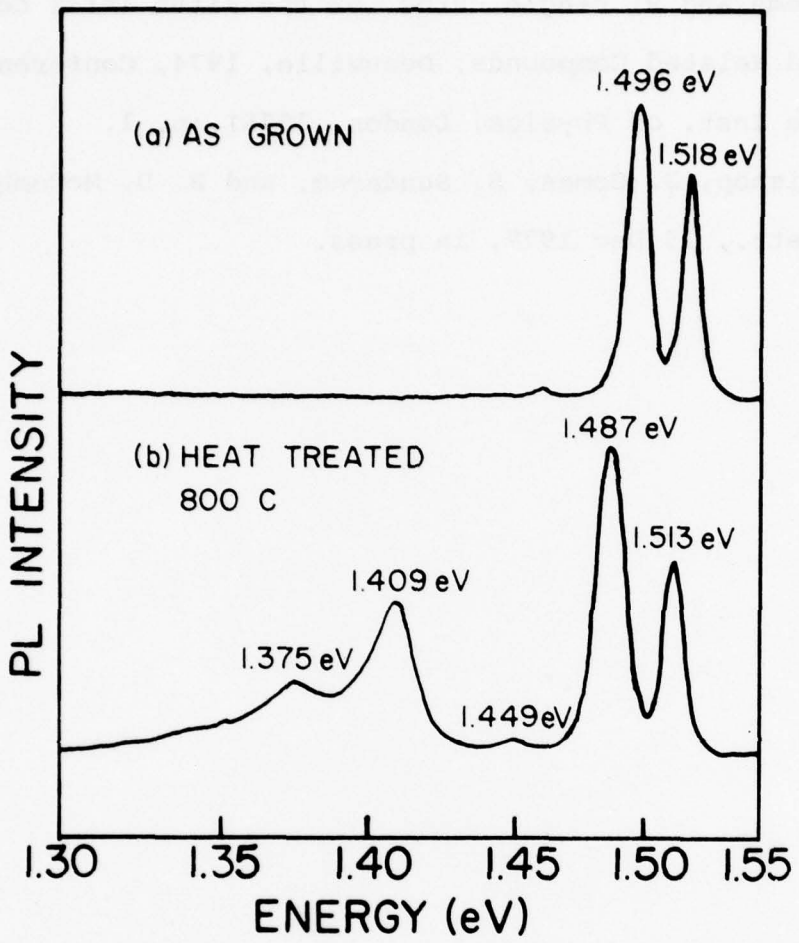

Fig. 19 — Low temperature PL spectra for n-type bulk Si-doped GaAs: a) before heat treatment and b) after a 30 minute anneal at 800°C in flowing H_2 gas

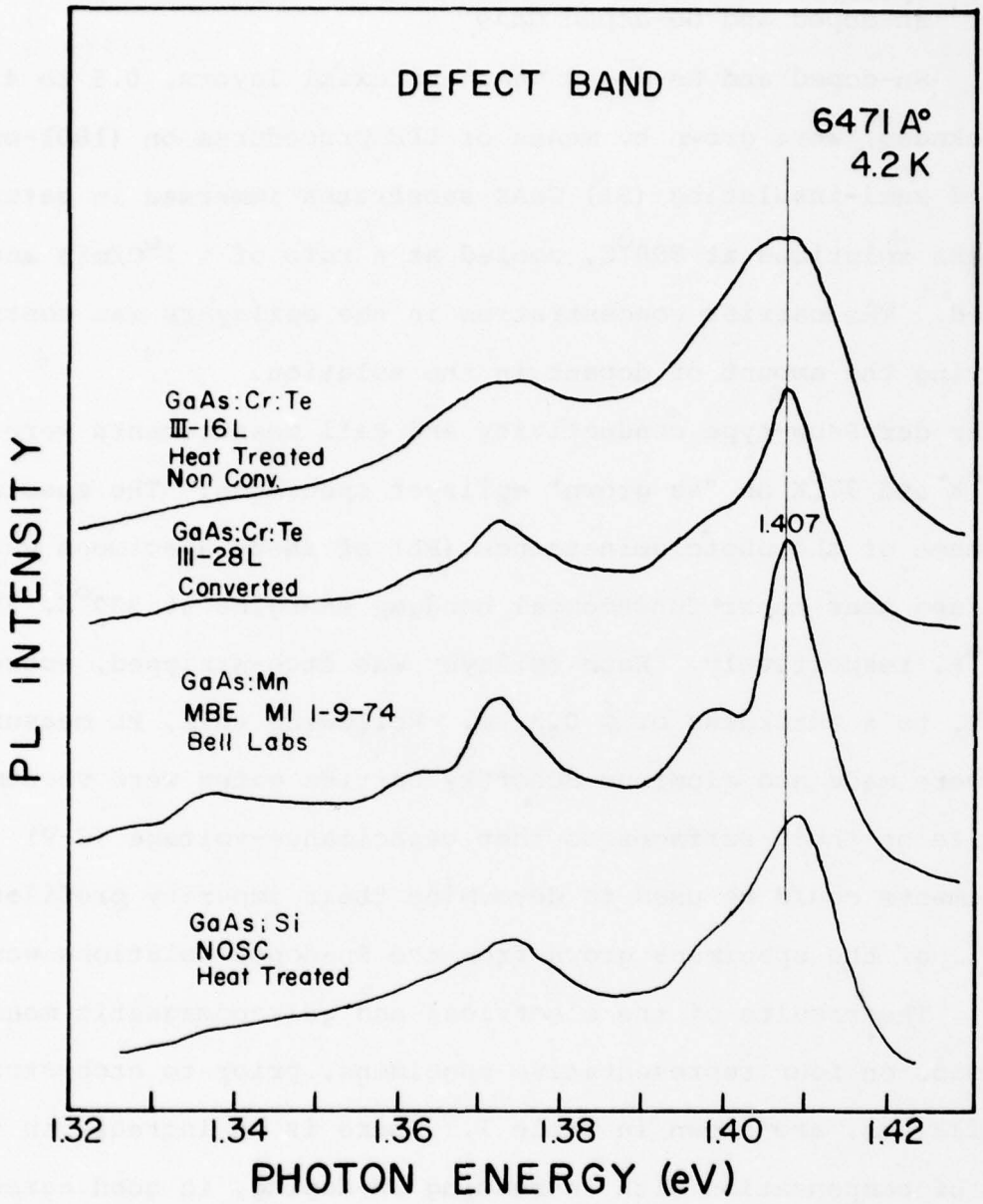

Fig. 20 — PL spectra in the region of the "defect" band for the four indicated GaAs samples. Samples III-16L and III-28L were annealed for 90 minutes at 740°C in flowing H_2 gas. The Si-doped GaAs was annealed for 30 minutes at 800°C.

3. Epilayer-substrate Interfaces of Sn-doped and Ge-doped GaAs

Sn-doped and Ge-doped GaAs epitaxial layers, 0.5 to 4.0 μm in thickness, were grown by means of LPE procedures on (100)-oriented, Cr-doped semi-insulating (SI) GaAs substrates immersed in saturated Ga + GaAs solutions at 800°C, cooled at a rate of ∿ 1°C/min and decanted. The carrier concentration in the epilayers was controlled by varying the amount of dopant in the solution.

Van der Pauw-type conductivity and Hall measurements were made at 300°K and 77°K on "as grown" epilayer specimens. The spectral dependence of the photoluminescence (PL) of these specimens was determined near their fundamental bandgap energies at 300°K, 77°K, and 20°K, respectively. Each epilayer was etch-stripped, subsequently, to a thickness of $\lesssim$ 0.3 μm. Following this, PL measurements were made and aluminum Schottky barrier gates were vacuum--deposite on their surfaces so that capacitance-voltage (C-V) measurements could be used to determine their impurity profiles.

All of the specimens grown from the Sn-doped solutions were n-type. The results of the electrical and galvanomagnetic measurements made on four representative specimens, prior to etch-stripping the epilayers, are shown in Table I. There is an increase in the degree of compensation with increasing Sn-doping, in good agreement with the analysis and data of Wolfe and Stillman[1] on self-compensation of group IV impurities incorporated into GaAs.

The Sn donors are presumed to occupy Ga sites substitutionally: $Sn^{\ell} + V_{Ga} \rightleftharpoons Sn^{+}_{Ga} + e^{-}$. Its ionization energy has been identified

by Fetterman et al.[2] using an optically-pumped submillimeter NH_3 laser as 5.820 meV.

Figure 21 represents the 20°K PL spectral response of the 2.35 at. % Sn-doped epilayer. It shows a broad emission line at 1.518 eV which includes the exciton and shallow Sn donor-to acceptor or valence band transition. Also shown is a spectral peak at 1.493 eV previously identified in undoped epilayers[3,4] as a free to bound radiative recombination transition for a shallow carbon-on-arsenic site, C_{As}, acceptor. The PL spectral peak at 1.413 eV and its LO phonon replica at 1.377 eV are attributed to an arsenic vacancy-acceptor complex, localized at the epilayer-substrate interface.[3,4] These spectral peaks are produced by the thermally-induced degradation of the substrate surface within an LPE reactor prior to epitaxial growth; Fig. 22 shows that these same peaks appear as well at the interface of undoped GaAs layers grown under similar conditions from a Ga + GaAs solution. The three spectral peaks at 1.36 eV, 1.32 eV, and 1.29 eV, whose position, intensity and bandwidth increased with Sn-doping, are attributed to Sn_{As} acceptors. They are consistent with the PL spectra found by Kressel et al.[5] in Sn-doped LPE-grown GaAs and are also in agreement with PL investigations of Schairer and Grobe[6] and of Schairer et al.[7] made at 77°K, 20°K, and 4.2°K which indicate that for $T \leq 20°K$ the free electron-to-acceptor or bound electron-to-acceptor transition corresponds to a PL peak at 1.35 eV with a binding energy of 167 meV and with two phonon replicas at 1.31 eV and 1.28 eV. The issue whether the Sn acceptor is a simple substitutional Sn_{As} or, as suggested by Panish,[8] a complex of the form $Sn_{As} \cdot 2V_{Ga}$ is not resolved.

A comparison of Sn-doped and undoped epilayers, Figs. 21 and 22, shows that the spectral peaks attributed to the arsenic vacancy-acceptor complex and its phonon replicas are smaller by a factor $\sim$ 20 in the Sn-doped layers. We attribute this to a partial compensation of these deep-level acceptors by shallow Sn donors diffusing into Ga vacancies which are generated by the thermal degradation of the substrate surfaces prior to the growth of the epilayers.[9] In order to test this assumption the epilayers were subjected to an anodization etch-stripping process which reduced their effective thickness to $d \leq 0.3$ μm. Figure 2 shows the 20°K PL spectrum of such an etch-stripped epilayer grown from a 2.35 at. % Sn-doped Ga + GaAs solution; the spectral peaks of Fig. 21 associated with Sn acceptors are absent in Fig. 23 indicating that self-compensation of the shallow Sn donors by Sn acceptors occurs within the epilayer and not at its interface. The remaining PL peaks are those corresponding to the arsenic vacancy deep-level acceptor complex at the epilayer-substrate interface. Their intensity decreases with increasing Sn-doping in the etch-stripped layers.

All the Ge-doped epilayers were determined to have p-type conductivity, suggesting that Ge is incorporated primarily as a substitutional acceptor by occupying an As site: $Ge^{\ell} + V_{As} \quad Ge^{-}_{As} + h^{+}$, in contrast with Sn which is incorporated as a donor for the same growth temperature. The electronic parameters of some representative specimens are listed in Table II.

Figure 24 shows the 20°K PL spectral response of a GaAs LPE layer grown from a solution containing 0.036 at. % of Ge. The most

dominant PL peak appears at 1.483 eV which can be attributed to the free-to-bound transition produced by the capture of a free electron by a neutral acceptor center created by a Ge atom occupying an As site, Ge_{As}.[10] It has a phonon replica at 1.447 eV. The usual PL peak due to the recombination of excitons observed in undoped and Sn-doped LPE layers is observed at 1.517 eV. The PL spectral peak at 1.412 eV previously observed in epilayer structures not doped with Ge, however, is observable only if much higher sensitivity is used. This may be due to the long absorption tail which is typical in p-type GaAs[11] as well as the reduction of vacancies at the interface due to their occupancy by Ge atoms.

To investigate the interface properties further, the epilayer was removed by anodization and etch-stripping. Figure 25 shows the PL spectrum of such an interface. The near-bandgap emission includes peaks at 1.517 eV due to exciton recombination, 1.493 eV due to the shallow C_{As} acceptor, and a shoulder at 1.481 eV due to the presence of Ge_{As} at the interface. The As vacancy-acceptor complex PL peak at 1.413 eV can now be observed since it no longer has to pass through the epilayer and be absorbed by it. The intensity of this deep level acceptor peak is approximately an order of magnitude lower than in undoped epilayers and comparable to Sn-doped epilayers in which cross-compensation takes place at the interface. In this case, Ge atoms occupy the thermally-generated As vacancies (as manifested by the presence of the 1.481 eV emission peak) and therefore the formation of As vacancy-acceptor complexes at the interface is suppressed.

TABLE I.

% at. Sn in melt	Epilayer thickness (μm)	Carrier concentration $n = N_d - N_a$ (cm^{-3})		Electron mobility μ (cm^2/V-sec)		N_d (cm^{-3})	N_a (cm^{-3})	N_d/N_a	Segregation coefficient of Sn $k=(N_d+N_a)/X^{\ell}_{Sn}$
		n (300°K)	n (77°K)	μ(300°K)	μ(77°K)				
0.34	2.1	$3x10^{16}$	$2.3x10^{16}$	4980	9660	$3.9x10^{16}$	$1.6x10^{16}$	2.5	$3.6x10^{-4}$
1.16	1.5	$1.1x10^{17}$	$8.7x10^{16}$	3300	4250	$1.7x10^{17}$	$8.7x10^{.6}$	2.0	$5.1x10^{-4}$
2.35	0.9	$1.4x10^{17}$	$1.3x10^{.7}$	3520	3810	$3.1x10^{17}$	$1.7x10^{.7}$	1.8	$4.6x10^{-4}$
3.46	1.2	$2x10^{17}$	$1.9x10^{17}$	3980	4040	$5.6x10^{17}$	$3.7x10^{17}$	1.5	$6.3x10^{-4}$

TABLE II.

at. % Ge	d(μm)	p(300°K) (cm^{-3})	p(77°K) (cm^{-3})	μ(300°K) (cm^2/V-sec)	μ(77°K) (cm^2/V-sec)
0.036	4.0	9.6×10^{16}	1.0×10^{16}	270	1755
0.10	3.0	2.8×10^{17}	2.3×10^{16}	173	776
0.19	1.8	4.7×10^{17}	5.2×10^{16}	185	386
0.39	1.6	1.0×10^{18}	2.9×10^{17}	150	123
0.87	2.4	1.6×10^{18}	5.2×10^{17}	119	93
1.9	3.0	4.0×10^{18}	7.5×10^{18}	78	27
3.2	1.4	7.4×10^{18}	1.3×10^{19}	55	36

References:

1. C. M. Wolfe and G. E. Stillman, Appl. Phys. Lett., 27, 564 (1975).
2. H. R. Fetterman, J. Waldman, C. M. Wolfe, G. E. Stillman and C. D. Parker, Appl. Phys. Lett., 21, 434 (1972).
3. W. Y. Lum, H. H. Wieder, W. H. Koschel, S. G. Bishop and B. D. McCombe, Appl. Phys. Lett., 30, 1 (1977).
4. W. H. Koschel, S. G. Bishop, B. D. McCombe, W. Y. Lum and H. H. Wieder, in Proc. International Symposium on Gallium Arsenide and Related Compounds (Univ. of Edinburgh, Scotland, 1976), p. 98.
5. H. Kressel, H. Nelson and F. Z. Hawrylo, J. Appl. Phys., 39, 5647 (1968).
6. W. Schairer and E. Grobe, Solid State Commun., 8, 2017 (1970).
7. W. Schairer, D. Bimberg, W. Kottler, K. Cho and M. Schmidt, Phys. Rev., B13, 3452 (1976).
8. M. B. Panish, J. Appl. Phys., 44, 2659 (1973).
9. S. Y. Chinag and G. L. Pearson, J. Appl. Phys., 46, 2986 (1975).
10. W. Schairer and W. Graman, J. Phys. Chem. Solids, 30, 2225 (1969).
11. H. C. Casey, Jr., D. D.Sell and K. W. Wecht, J. Appl. Phys., 46, 250 (1975).

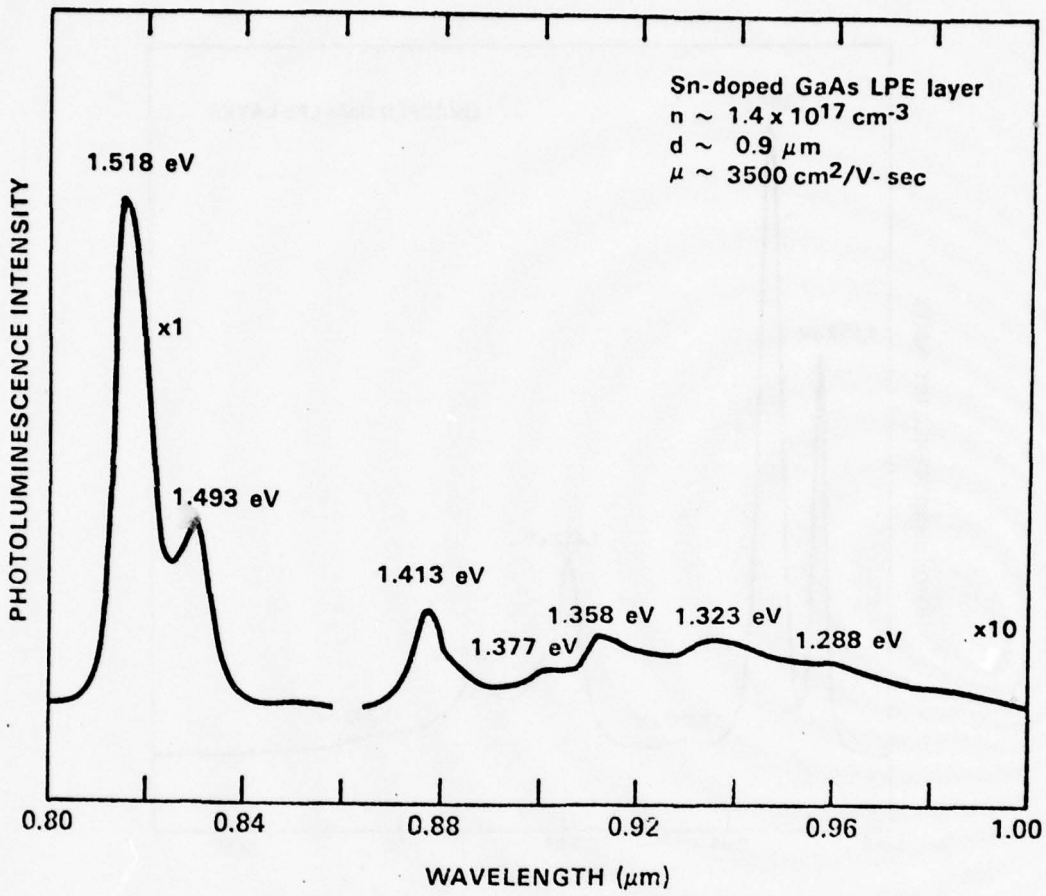

Fig. 21 — PL spectral response at 20°K of an epilayer grown from a 2.35 at. % Sn-doped solution

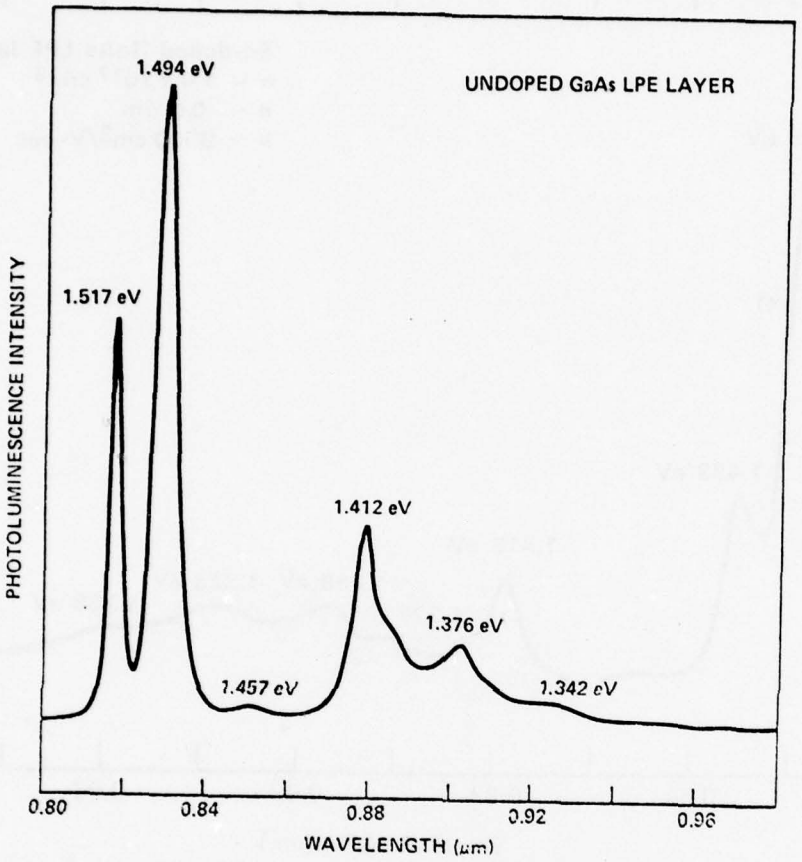

Fig. 22 — Similar data for an undoped epilayer

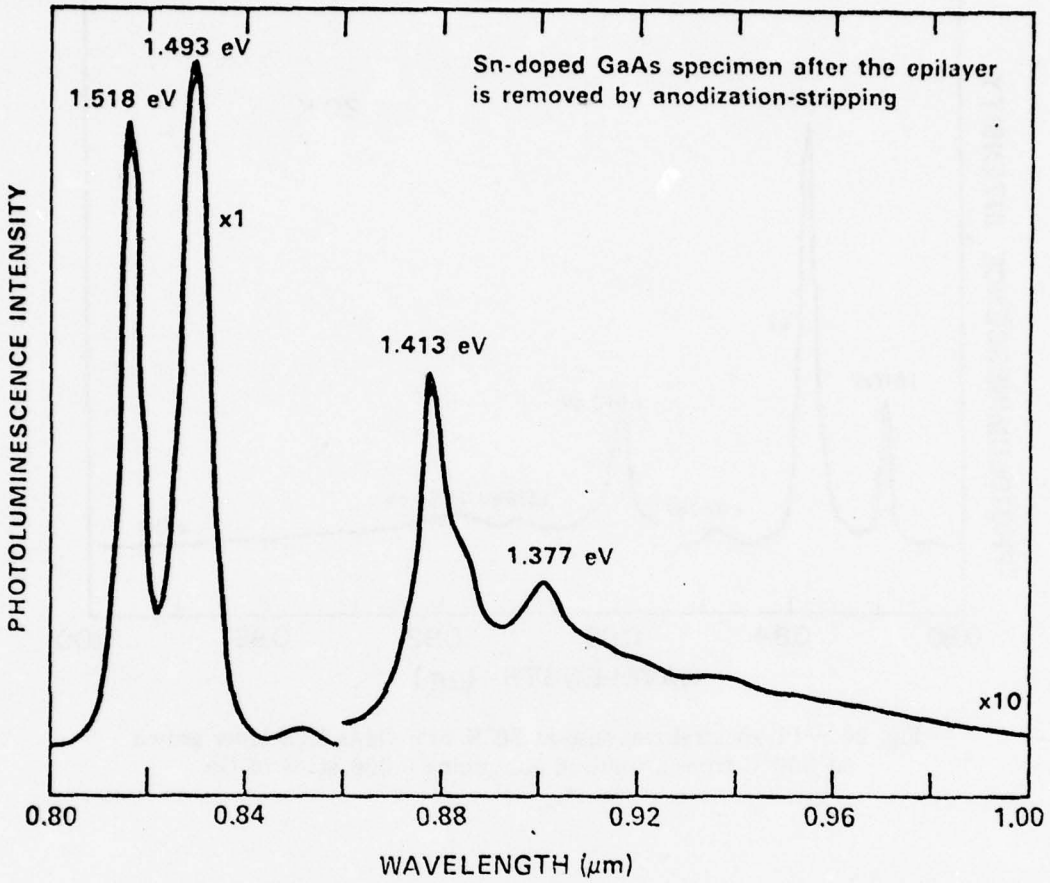

Fig. 23 — PL spectral response at 20°K of a specimen in which the Sn-doped epilayer has been removed by anodization etch-stripping

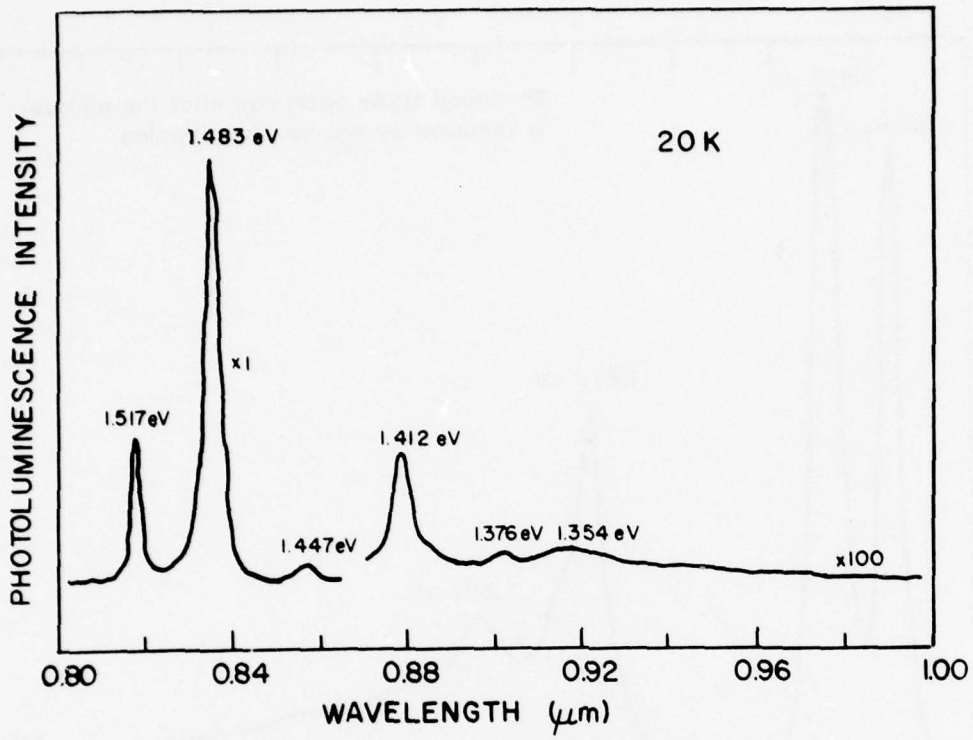

Fig. 24 — PL spectral response at 20°K of a GaAs LPE layer grown at 800°C from a solution containing 0.036 at. % of Ge

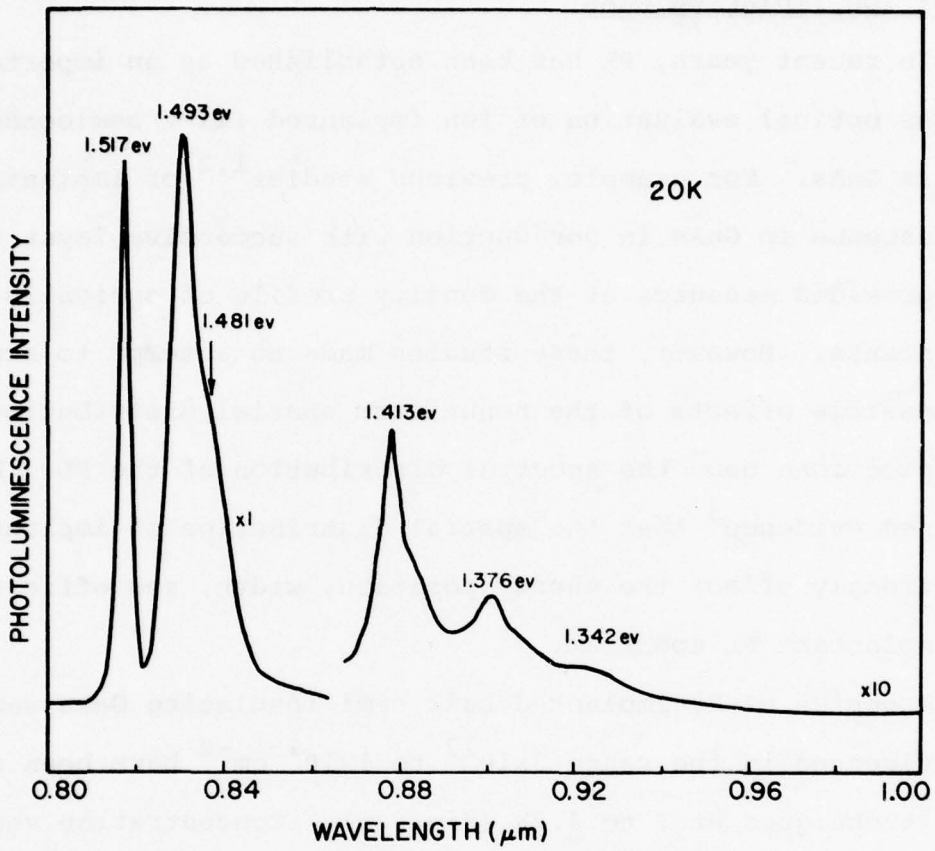

Fig. 25 — PL spectrum at 20°K of the epilayer-substrate interface of a Ge-doped GaAs specimen

D. Photoluminescence Characterization of Ion Implanted GaAs

In recent years, PL has been established as an important tool for the optical evaluation of ion implanted III-V semiconductors such as GaAs. For example, previous studies[1,2] of implantant luminescence in GaAs in conjunction with successive layer removal have provided measures of the density profile of optically active implantants. However, these studies made no attempt to account for the possible effects of the nonuniform spatial distribution of the implanted ions upon the spectral distribution of the PL. We have obtained evidence[3] that the spatial distribution of implanted ions can strongly affect the energy position, width, and efficiency of the implantant PL spectrum.

A series of Be-implanted bulk semi-insulating GaAs samples with fluences in the range 3×10^{12} to $1\times10^{15}cm^{-2}$ have been studied by PL techniques at 2 to 4.2K (Fig. 26). Concentration versus depth profiles of Be implanted into GaAs at 100 keV obtained by secondary-ion mass spectroscopy (SIMS) techniques have shown that the implanted distribution is in agreement with the Gaussian LSS theoretical distribution centered around 3200 Å. In relatively low fluence samples ($<10^{14}cm^{-2}$) this distribution is not altered significantly by the post-implantation anneal. However, in high fluence samples ($>10^{14}cm^{-2}$) the Be ions undergo an anomalous redistribution during the anneal in which a high atomic concentration ($>10^{19}cm^{-3}$) occurs in the surface region and a relatively flat plateau in the distribution with concentration $\sim5\times10^{18}cm^{-3}$ extends

nearly 6000 Å into the sample.[4] While these differences in implantant depth distribution for the high and low fluence samples of Be implanted GaAs do not manifest any obvious effects upon the PL spectra of Fig. 1, we will show that studies of the PL as a function of penetration depth and intensity of the exciting light can be interpreted in terms of these distributions.

At high fluence, the conduction band to Be acceptor PL transition (free-to-bound or FB) exhibits an anomalously large shift in its energy as a function of exciting light intensity (Fig. 27(a)). This shift has been explained in terms of an optical profiling of the depth dependent Be implantant concentration with changing excitation intensity. If it is assumed that the diffusion length of photoexcited carriers in the implanted layer is small in comparison to the layer thickness, the density of photoexcited carriers at a given depth in the layer will be a function of the incident intensity of the exciting light and the absorption coefficient at the wavelength of the exciting light. Light of wavelength 6471 Å will be attenuated by a factor of 1/e at a penetration depth of about 3000 Å in GaAs. If it is assumed that there is some minimum intensity of exciting light which must reach a point in the crystal in order to excite an observable luminescence from that depth, clearly this minimum intensity level will reach farther into the crystal as the incident light intensity is increased. This means that in the limit of little or no carrier diffusion low excitation levels will produce luminescence which is characteristic of recombination centers near the sample surface; as the exciting light

intensity is increased, the photoexcited carrier distribution reaches recombination centers which lie deeper in the crystal. If the PL spectrum from the centers lying near the surface differs from that which characterizes the centers lying deeper in the sample, this difference will manifest itself as a change in the observed PL spectrum as a function of excitation intensity as seen in Fig. 27(a).

Supporting evidence for this interpretation is provided by the PL spectra presented in Fig. 27(b). The two spectra were obtained with exciting light of differing wavelength but identical intensity (0.75 W/cm^2). The 4762 Å (blue) light is more highly absorbed than the 6471 Å (red) light and accentuates radiative recombination centers (Be implantants) within about 1000 Å of the sample surface (in the limit of no diffusion). Correspondingly the red light reaches Be atoms lying much deeper in the sample. Note that the direction and magnitude of the spectral shift between the PL spectrum excited by the highly absorbed blue light and that excited by the more deeply penetrating red light corresponds to that of the shift which was produced with increasing excitation intensity (Fig. 27(a)). The low intensity spectrum of Fig. 27(a) and the spectrum of Fig. 27(b) excited by blue light are both characteristic of the Be atoms in the high density atomic concentration region ($>10^{19} cm^{-3}$) near the surface of this high fluence implanted layer; conversely, the high intensity spectrum of Fig. 27(a) and the spectrum of Fig. 27(b) excited by red light are dominated by PL originating from Be centers lying deeper in the sample which are characteristic of the

$\sim 5 \times 10^{18} cm^{-3}$ concentration of the plateau of the distribution. The peak energy and width of the shallow acceptor PL band are strongly dependent upon acceptor concentration[5] at these relatively high concentrations (10^{18}-$10^{19} cm^{-3}$); hence the observed PL band shifts in energy as Be acceptors in spatial regions of different concentrations dominate the PL spectrum. This interpretation is consistent with the fact that the energy of the peak of the high power and red light excited PL spectra are in good agreement with the previously reported 1.493 eV value for the F-B transition in Be implanted GaAs.[1-2]

While it has been suggested that post-implantation annealing restores carrier diffusion lengths to the $\sim$ 1 μm values characteristic of unimplanted crystals, the occurrence of these profiling effects in implanted layers $\sim$ 5000 Å thick implies that the diffusion lengths of photoexcited carriers in annealed implanted layers in bulk substrates are in fact much less than 1 μm.

In addition, a series of epitaxial samples of GaAs implanted with Be to a fluence of $5 \times 10^{12} cm^{-2}$ and annealed at temperatures ranging from 250°C to 800°C have been studied by PL techniques. These measurements have demonstrated the existence of a threshold for the appearance of efficient Be shallow acceptor PL at an annealing temperature of $\sim$ 450°C (Fig. 28). This corresponds closely to the annealing threshold for electrical activity of implanted Be in GaAs. Possible evidence for the observation of a donor-acceptor pair radiative transition associated with the implanted Be acceptors has been obtained in these epitaxial samples.

References:

1. P. K. Chatterjee, Ph.D. Thesis, University of Illinois (1976). Available from NITS, Springfield, VA (Report #ADA-025-607).
2. J. Comas, L. Plew, P. K. Chatterjee, W. V. McLevige, K. V. Vaidyanathan, and B. G. Streetman, Ion Implantation in Semiconductors and Other Materials, edited by F. Chernow (Plenum Press, NY, 1977) in press.
3. S. G. Bishop, J. Comas, S. Sundaram, and B. D. McCombe, Appl. Phys. Lett. (15 Dec 1977, in press).
4. J. Comas and L. Plew, J. Elect. Mat. 5, 209 (1976).
5. J. I. Pankove, Optical Processes in Semiconductors (Prentice-Hall, Inc., Englewood Cliffs, NJ, 1971) pp. 134-136.

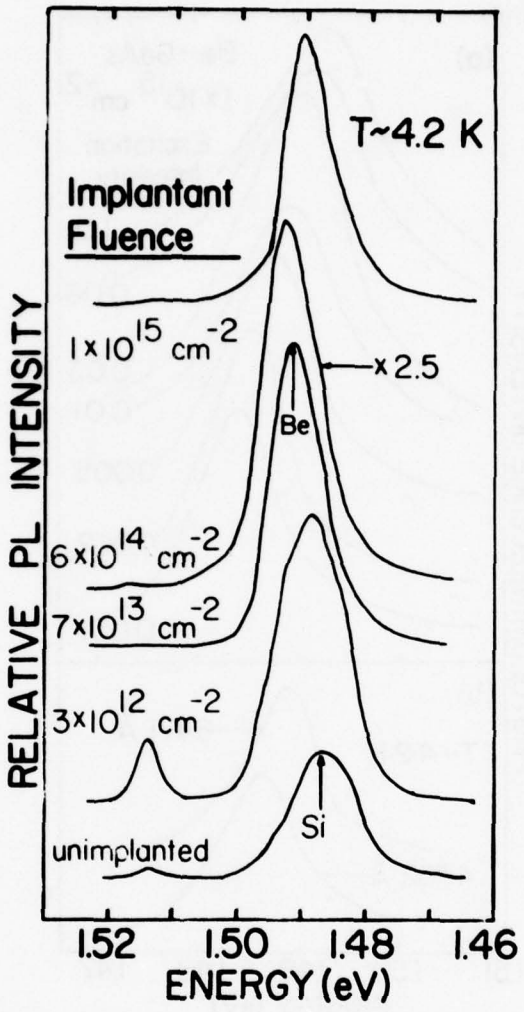

Fig. 26 — Photoluminescence spectra from bulk chromium doped GaAs samples implanted with 100 keV Be ions at a range of fluences and annealed at 800°C with SiO_2 encapsulation. Excitation was provided by the 6471 Å line of a K^+ laser.

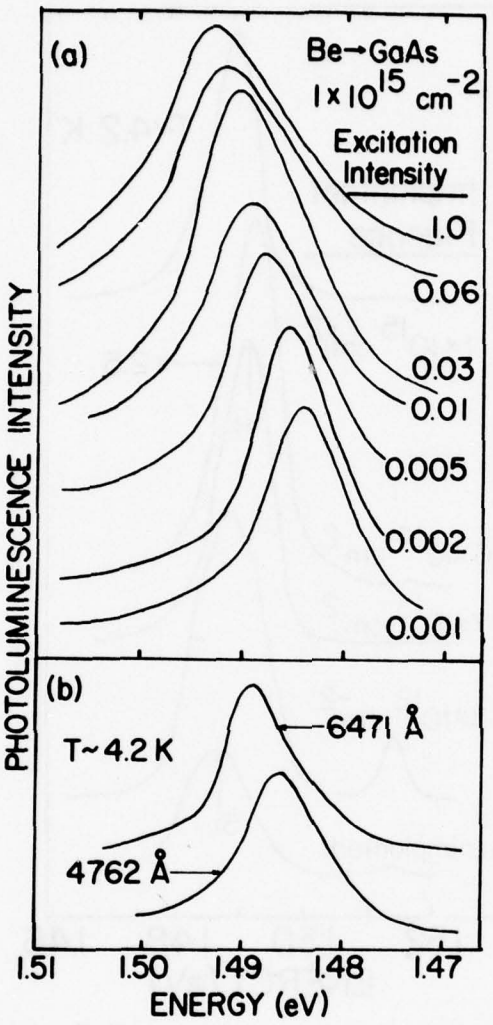

Fig. 27 — (a) Photoluminescence spectra from shallow acceptors in GaAs implanted with a $1x10^{15}cm^{-2}$ fluence of Be for a four decade range in the intensity of the 6471 Å exciting light. (b) Photoluminescence spectra for the same sample excited by 6471 Å and 4762 Å light of equivalent power ($\sim$ 0.75 W/cm^{-2}).

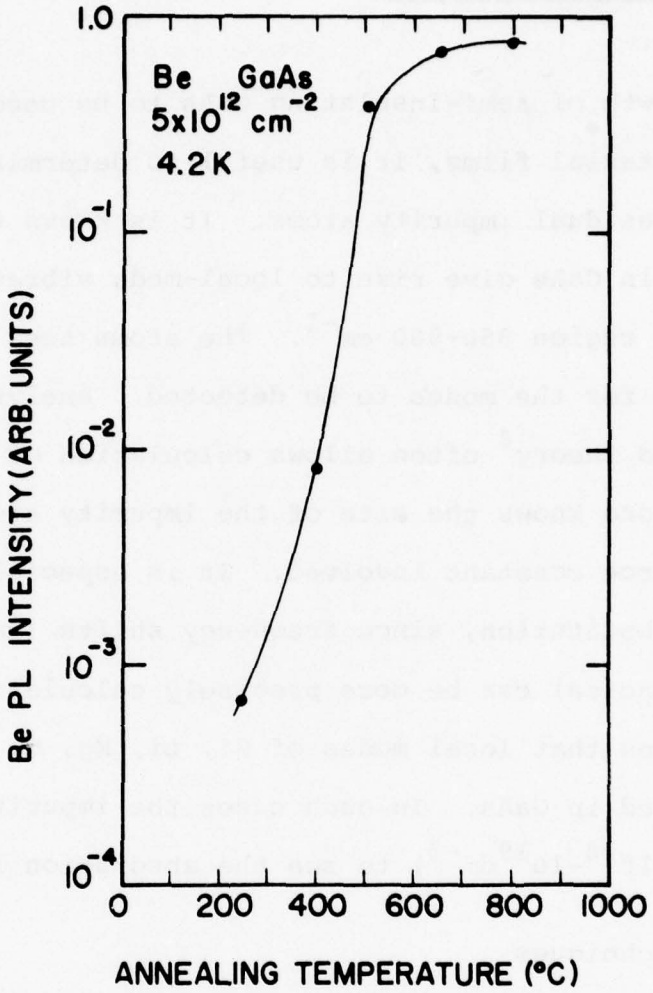

Fig. 28 — Intensity of Be shallow acceptor photoluminescence from epitaxial GaAs implanted with Be to a fluence of $5 \times 10^{-12} cm^{-2}$, as a function of post-implantation annealing temperature.

E. Infrared Local Vibrational Mode Spectroscopy of Boron Impurities in GaAs

Introduction

In the growth of semi-insulating GaAs to be used as substrates for epitaxial films, it is useful to determine the type and number of residual impurity atoms. It is known that light impurity atoms in GaAs give rise to local-mode vibration lines[1-7] in the spectral region 350-800 cm^{-1}. The atoms need not be electrically active for the modes to be detected. Analysis based on well-established theory[8] often allows calculation of the frequency of the mode if one knows the site of the impurity atom and can estimate the force constant involved. It is especially useful to use isotopic substitution, since frequency shifts (rather than absolute frequencies) can be more precisely calculated. The literature[1-7] indicates that local modes of Si, Li, Mg, C, B, P and Al have been studied in GaAs. In such cases the impurity densities are made high (10^{18}-$10^{19}cm^{-3}$) to see the absorption lines more easily.

Experimental Techniques

We have developed a two-beam infrared transmission system which allows the measurement of the difference in transmission between two samples of GaAs. The imageof a globar source is split by a chopper, so that the top half is chopped 180^{o} out of phase with the bottom half. The radiation is sent through a grating monochromator and refocused after the exit slit. At this point two samples are abutted in a dewar, so that the upper and lower halves of the focused image pass through the top and bottom samples, respectively. The radiation is

finally focused at a Cu:Ge photoconductive detector. By careful adjustment, it is possible to have the two beams cancel out at a spectral frequency where the samples are identically transparent. Then any difference in transmission (absorption) at another spectral frequency shows up as a positive or negative signal after lock-in-amplifier detection depending on which sample is absorbing. Typically, at a null setting, the gain may be increased one to two orders of magnitude to amplify differences between the two samples. Intrinsic optical-phonon absorption common to both samples cancels out, making the search for local-mode vibration lines easier.

Sample Characteristics

Two samples were measured by this technique. They were cut from opposite ends of the same boule, which was grown by liquid encapsulation in boric oxide by the Czochralski method (S. H. Lee, Code 5221). One sample was n-type with $n \sim 10^{10} cm^{-3}$ and the other was p-type with $p \sim 10^{13}$-$10^{14} cm^{-3}$. Presumably, they were highly compensated and contained a much higher density of impurities than the transport measurements imply. Because of the way the crystal was pulled, it is believed that the p-type sample contained much more boron than the n-type sample. However, it is not understood why the present samples switched type from n to p from the top to bottom of the boule, or what impurities produce the electrical properties. A rough estimate of the boron content was made by spark-source mass-spectroscopy techniques and was found to be

$\sim 4 \times 10^{16} cm^{-3}$ ($\sim$ 1 ppm). Other light impurities identified in lesser amounts were Na, Mg, Al, K, and Ca. Because of the low carrier density, negligible free-carrier absorption is present in these samples. Therefore, it is not necessary to electron-irradiate the samples to remove the free-carrier absorption.[1-7]

Results and Discussion

Due to the fact that the path lengths in the two beams are not exactly identical, absorption lines due to water vapor were always observed. We attempted to dry the optical path but could not dry sufficiently to eliminate these absorption lines. The magnitude of differential absorption was small, but turned out to be comparable to the other absorption lines seen which we assigned to B.

The transmittance of the boron-containing sample of GaAs in the spectral region of interest is shown in Fig. 29(a). The samples were 1.07 mm thick and were cooled to near-liquid-nitrogen temperature. The multiphonon bands of GaAs are indicated by arrows, while the sharper lines are due to water-vapor absorption. The single-beam spectrum of the other sample with much less B is nearly identical (but reversed in sign on the x-y recorder trace) to within the noise level. The background spectrum with the dewar removed from the beam is shown also. The absolute transmittance of GaAs at 590 cm^{-1} is $\sim$ 0.48. However, when the difference spectrum is recorded with a substantial gain increase, the results shown in Fig. 29(b) are obtained. Two spectra are shown, the upper one for an undried

optical path and a gan of x20 and the lower one for a dried optical path and a gain of x50. Two prominent features are seen at 516 and 538 cm^{-1} which agree very closely in position with literature values[1] of the local modes assigned to B (517.0 and 540.2 cm^{-1}). These two lines are assigned to B^{11} and B^{10} on Ga sites with the natural abundance being 4 to 1. Thus, the line at 516 cm^{-1} should be four times more intense. When the background level of radiation determined by the intrinsic phonon absorption at the centers of the two lines is considered, the lower-frequency line is really somewhat stronger than the higher-frequency line. However, it is difficult to determine a four-to-one ratio.

Between the two lines is another structure. A phonon line of GaAs does occur at 528 cm^{-1} with an absorption coefficient[7,9] of 35 cm^{-1} which can show up if the two samples are not the exact same thickness.[1] Our samples differed in thickness by at most 0.02 mm (as determined with a micrometer), and we estimate that this line might be comparable in size to the feature seen. Differential absorption of water vapor is down (negative), while the absorption credited to B is up (positive). We can thus tell which beam is slightly longer and which sample is absorbing. The structure at 516 and 538 cm^{-1} is caused by the sample which contains the greater amount of B. Due to instrumental artifacts, the background level is not horizontal. The dotted line in Fig. 29(b) is our estimate of the background if neither water vapor nor B in GaAs were absorbing. A search of the spectrum from 440 to 800 cm^{-1} revealed no other line structure which could not be attributed to water vapor

or background instrumental features. Three lines of water vapor near 575 cm^{-1} do seem to change shape somewhat upon partial drying, but at the moment we cannot definitely establish an absorption feature in one of the samples. The sensitivity of the measurement drops significantly at frequencies below 570 cm^{-1} because the intrinsic absorption in GaAs reduces the intensity drastically.

We have estimated the absorption coefficient of the line at 538 cm^{-1} to be $\sim$ 0.3 cm^{-1}. This is superimposed on the intrinsic absorption coefficient of 15 cm^{-1}. We can correlate this with the B content of $\sim 4 \times 10^{16} cm^{-3}$ and estimate that our ultimate sensitivity might be as low as 0.1 cm^{-1} ($\sim 1 \times 10^{16} cm^{-3}$). For B in Si-doped GaAs with $\sim 1 \times 10^{18}$ carriers/cm^3, the product of absorption coefficient and line width is $\sim$ 10 cm^{-2} for the line at 540.2 cm^{-1}. The width of this line[1] is $\sim$ 3 cm^{-1} which gives an absorption coefficient of $\sim$ 3.3 cm^{-1}. Extrapolating our results implies that this Si-doped sample contain $\sim 4 \times 10^{17}$ atoms/cm^3 which is comparable to but slightly less than the Si content. Boron is presumably electrically inactive, and so its presence cannot be determined by electrical transport measurements.

In the literature, B absorption has been seen in Si-doped ($10^{18} cm^{-3}$) GaAs grown by liquid encapsulation in boric oxide.[2-4] The Si is presumed to react with the oxide to produce B impurities along with the desired Si impurities. The two lines we see are credited to B on Ga sites B(Ga) but a number of other weaker lines are also seen[2,3] and are assigned to B on As sites B(As) and a variety of B(Ga)-Si(As) complexes, in addition to lines of Si itself. One line at 601.4 cm^{-1} appears comparable in intensity to the line

at 540.2 cm^{-1} and is assigned to B(As). We see no line at this frequency. Our samples presumably do not have such a rich spectrum of absorption lines, since no deliberate doping was done in growing this semi-insulating sample. Since both the samples we used probably have the same number of impurities except for B, we would not see other impurity lines by this technique which cancels features common to both samples.

Future Directions

To improve the present experiment, it is desirable to decrease the spectral slits to 2 cm^{-1} rather than the present 4 cm^{-1}, so as to discriminate better the sharper water-vapor lines from the wider local-mode lines. Also, the optical path should be dried more effectively, perhaps by purging with nitrogen gas from a liquid-nitrogen dewar. Another factor-of-two more signal could be obtained by alternating the entire globar image between each sample by a somewhat different chopping scheme. This would also reduce the effects of certain instrumental artifacts which complicate the spectra. With such improvements, the present limits of sensitivity could be lowered substantially.

Acknowledgements

The samples were grown and characterized by S. H. Lee, Code 5221. Assistance in some of the experimental aspects of this work was obtained from R. T. Holm and N. Ginsburg, Code 5233.

REFERENCES:

1. R. C. Newman, F. Thompson, H. Hyliands and R. F. Peart, "Boron and Carbon Impurities in Gallium Arsenide," Solid State Comm. 10, 505-507 (1972).
2. F. Thompson and R. C. Newman, "Localized Vibrational Modes in Gallium Arsenide Containing Silicon and Boron," J. Phys. C: Solid State Phys. 5, 1999 -2010 (1972).
3. S. R. Morrison, R. C. Newman and F. Thompson, "The Behavior of Boron Impurities in n-type Gallium Arsenide and Gallium Phosphide," J. Phys. C: Solid State Phys. 7, 633-644 (1974).
4. K. Laithwaite, R. C. Newman, J. F. Angress and G. A. Gledhill, "Boron Acceptor Centers in Silicon-doped LEC Gallium Arsenide," in Gallium Arsenide and Related Compounds (Edinburgh), 1976, ed. by C. Hilsum, Conference Series Number 33a, The Institute of Physics, Bristol 1977, pp. 133-140.
5. P. C. Leung, L. H. Skolnik, W. P. Allred and W. G. Spitzer, "Infrared Absorption Study of Li-diffused Mg-doped GaAs," J. Appl. Phys. 43, 4096-4104 (1972).
6. L. H. Skolnik, W. G. Spitzer, A. Kahan and R. G. Hunsperger, "Infrared Localized-Vibrational-Mode Absorption in Ion Implanted Aluminum and Phosphorous in Gallium Arsenide," J. Appl. Phys. 42, 5223-5229 (1971).
7. M. E. Levy and W. G. Spitzer, "Localized Vibrational Modes of Li Defect Complexes in GaAs," J. Phys. C: Solid State Phys. 6, 3223-3244 (1973).

8. I. F. Chang and S. S. Mitra, "Long Wavelength Optical Phonons in Mixed Crystals," Advances in Physics 20, 359-404 (1971).

9. W. Cochran, S. J. Fray, F. A. Johnson, J. E. Quarrington and N. Williams, J. Appl. Phys. 32, 2102-2112 (1961).

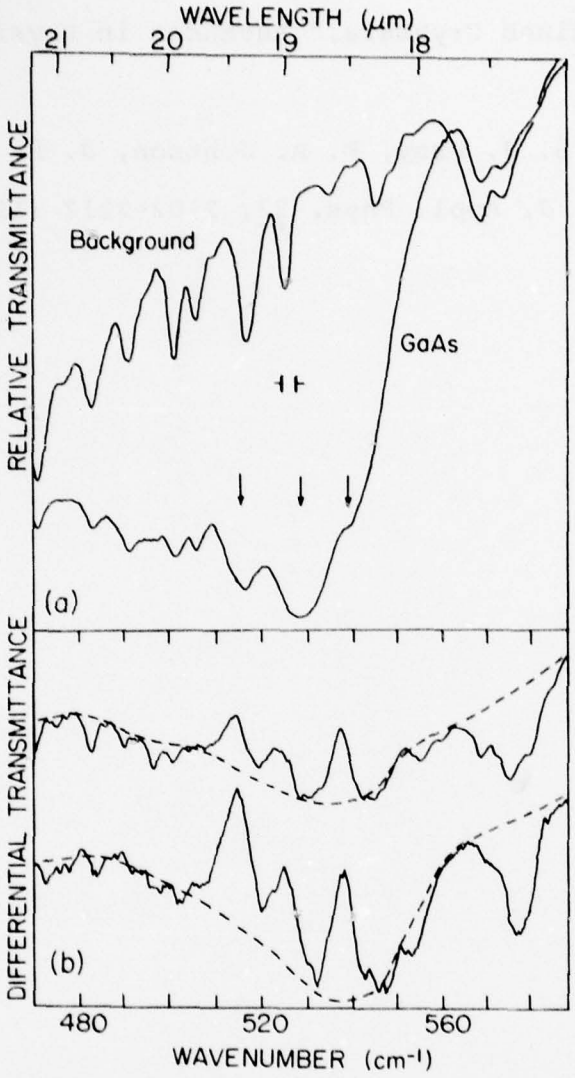

Fig. 29 — (a) The background spectrum due to the components of the spectroscopic system showing absorption lines of water vapor in the optical path. The spectrum of GaAs shows the transmittance of the boron-containing sample. Arrows indicate optical-phonon frequencies of GaAs. (b) The difference spectrum of the two samples of GaAs, one of which presumably contains much more boron than the other. The upper one is for an undried optical path and a gain of x20 over the GaAs spectrum in part a. The lower one is for a partially dried path and a gain of x50. The dashed lines are estimates of the spectrum if no water or boron were present. The dashed lines would be horizontal if no instrumental artifacts were present.

IV. DEVICE FABRICATION AND EVALUATION

A. Introduction

The purpose of this segment of the characterization program is to determine the relationship between GaAs material parameters and GaAs microwave device performance. The test vehicle used for this purpose is the gallium arsenide Schottky barrier field effect transistor (GaAs FET). The performance of this device is extremely sensitive to material parameters and at present there is no theory which relates FET performance to material growth and quality. There is an urgent need to tie FET performance to material parameters in order that GaAs material can be improved on a continuing basis. Fig. 1 shows how the GaAs FET fabrication effort is related to the overall NRL GaAs program. Samples grown in NRL 5220 are supplied to NRL 5270 for non-destructive analysis and then forwarded to NRL 5210 for FET fabrication (destructive test). Results are forwarded to NRL 5220 for continuous materials improvement. The interaction described in Fig. 1 is unique to the GaAs material/device community.

B. FET Fabrication

The FET geometry used for characterization is shown in Fig. 2. More detail of the device cross section is given in Fig. 3. The dimensional tolerances are related. The gate length, L_g, is between 1 and 2 microns with a corresponding source to drain spacing, L_{SD}, between 4 and 7 microns. Gate width Z, is 255 microns. In a few instances super relaxed geometry FETs were fabricated with L_g = 2-10 microns for the purpose of initiating new processing techniques and obtaining carrier concentration profiles for actual FET structures.

Processing of NRL FETs is accomplished by a combination of conventional contact photolithography and lifting processes for source, drain and gate metallizations. As shown in Fig. 3, the gate is Al and the source/drain ohmic contacts are sintered Au/Ge/Ni. All metallizations are resistance evaporated at a pressure at least $1x10^{-5}$ Torr. The specific contact resistance of the Au/Ge/Ni contacts after sintering at 450°C for 30 sec is $8\text{-}9x10^{-7}$ ohm-cm^2. In some instances, the channel region is recessed using a chemical etch. To aid in wire bonding and FET reliability the sintered source and drain contacts are overcoated with about 3000 Å of vacuum deposited gold after the gate is in place.

C. FET Characterization - Experimental

GaAs material is continuously characterized as it is being processed into FETs. After the FETs are completed extensive DC and RF testing is done. The entire characterization scheme is outlined in Fig. 4.

Two important evaluations occur during processing: determination of the carrier concentration profile and analysis of the source/drain DC I-V characteristic with gate absent. Fig. 5 shows a typical carrier concentration profile obtained from an automatic doping profile machine. Such a profile is commonly referred to as a n-x plot. The rejection criteria shown in Fig. 5 are predicated on results obtained by several commercial producers of GaAs FETs as well as results obtained at NRL. These results indicate that optimum performance of small signal GaAs FETs is obtained when the channel region thickness a' (see Fig. 3) is between 0.2 and

0.3 microns and the channel doping, N_D, is $1\text{-}2\times10^{17}cm^{-3}$. If the as-grown channel thickness, a_1, is more than 0.3 microns, the region beneath the gate must be recessed (as shown in Fig. 3) to achieve channel pinch-off and high transconductance. Also the carrier concentration must drop abruptly at the edge of the channel to prevent excessive current flow beneath the channel which increases the output conductance and the noise figure. Industrial results suggest that the lowest noise figure occurs when the n-x roll-off slope is less than 1000 Å/decade change in N_D.

After accepting a wafer on the basis of its n-x characteristics, it is processed to the point where only the isolation mesa and the sintered ohmic contacts are present as shown in Fig. 6(a). The I-V characteristic between the source and the drain is carefully measured and is of the form shown in Fig. 6(b). This curve yields a great deal of information about the quality of the ohmic contacts, the mobility of the channel and the interface between the channel and the material beneath it. Asymmetries in the I-V characteristic indicate either poor contacts or a poor interface. Material with an asymmetrical I-V characteristic is usually rejected as unsuitable for further FET processing. If the I-V curve is symmetric, the equations given in Fig. 6(b) are used to calculate the average channel low field mobility, μ_o, and the average channel saturated drift velocity, V_S. Ep is the peak electric field in the GaAs and R_c has been determined independently to be 2-3 ohms for properly sintered contacts.

After passing the source/drain I-V test, the FET wafer is completed by adding gates and a gold overlay to the source and drain. The three terminal DC I-V characteristics are carefully measured and checked for backside gating (hidden depletion layer), looping and light sensitivity. Fig. 7 indicates the experimental conditions for backside gating. In some instances, a profile of saturated channel velocity is determined using an unpublished technique developed at Varian Associates and shown in Fig. 8. Below is a list of static parameters measured on each FET.

I_{DSS} - drain current at zero gate voltage

g_m - small signal ac transconductance

V_p - pinchoff voltage

R_s - source resistance

R_d - drain resistance

I_{gr} - gate reverse leakage current

V_{gbd} - gate reverse breakdown voltage

R_s and R_d are measured by forward biasing the gate and noting the open circuit voltage appearing at the drain and the source, respectively.

FETs with attractive DC characteristics are scribed and mounted into microwave carrier packages for RF characterization. The following DC characteristics are considered attractive:

I_{ds} < 80 mA

V_p < 6 volts

g_m > 10 mmho

R_s > 10 ohms

Devices that loop, backgate, or show light sensitivity are not rejected. They are characterized at microwave frequencies and compared with those FETs which do not loop, backgate, or show light sensitivity. The RF measurements consist of insertion gain versus frequency and noise figure at specified I_D (drain current) levels.

D. Material Processed

About 60 wafers have been processed into FETs. The aproximate wafer breakdown is indicated below.

20 wafers (LPE) - NRL Code 5220

10 wafers (II) - NRL Code 5212

25 wafers (LPE, VPE) - Industrial Laboratories

5 wafers (LPE) - NOSC, Code 4640

Below is a listing of supplier, type of material and presence of a buffer layer:

NRL Code 5220 - LPE/No Buffer

NRL Code 5212 - Ion Implant/no buffer

NOSC Code 4640 - LPE/no buffer

Avantek - LPE/buffer

Raytheon - VPE/buffer

RCA - VPE/no buffer

Rockwell International - LPE/no buffer

Teledyne MEC - VPE/no buffer
VPE/buffer

Texas Instruments - VPE/buffer

Many laboratories use a buffer layer to improve FET performance. This buffer layer is grown on a GaAs semi-insulating substrate prior to channel growth. The buffer layer is typically about 10 microns thick and doped to $10^{13}cm^{-3}$ or less. Its purpose is to shield the channel layer from the semi-insulating substrate during the channel growth process. Without the buffer layer, the interface between the channel and the substrate can become degraded and limit FET performance. The physics of this degradation is not understood. However, the FET device community strongly feels that the interfacial degradation can be reduced with appropriate substrate material. Accordingly, NRL Code 5220 has produced high quality GaAs semi-insulating substrates to test this thesis. Code 5220 FET material contains no buffer layer and therefore forces the most stringent requirements on material quality.

E. FET Performance - Overall

During this reporting period NRL FET performance improved dramatically. The improvements are a result of process technology and improved material quality from both NRL Code 5220 and industrial sources. Fig. 9 shows the progress made in producing microwave FETs at NRL. At present, NRL Code 5210 is producing 1-2 micron gate length GaAs FETs with X-band gain performance equivalent to that achieved by industrial manufacturers. However, the noise figure of NRL GaAs FETs is about 2-3 db higher than that of commercially available devices. The higher noise figure appears related to the geometry of the NRL FETs. At present every attempt is being made to reduce the noise figure achieved with devices of

this geometry. Techniques employed to reduce the noise figure include thickening gate metallization, recessing the gate and in general reducing the source resistance, R_s. This troublesome parasitic reduces gain and increases noise figure. It is schematically shown in Fig. 10 along with other parasitics which reduce gain and increase noise figure. Typical values of R_s measured on NRL devices range from 6.5 to 10 ohms. An R_s value less than 5 ohms would be desirable. In addition, thickening the gate metallization should reduce the gate resistance, R_g (typically about 8-9 ohms) to about 5 ohms - a more acceptable value for low noise FETs.

New FET masks with a geometry which optimizes small signal microwave performance have been ordered. The new geometry is compared with the current geometry in Fig. 11. Both drawings are to the same scale. Note the shorter gate lengths and variable gate widths on the new masks. A variable gate width is desirable for purposes of impedance matching at various frequencies. Also the reduced size of the gate pad should decrease input capacitance. Included on the new FET mask are several test patterns for evaluating contact resistance, carrier concentration profile, Hall and drift mobility and deep levels.

The best NRL FET microwave performance results at 8 GHz are given in Table I. At this frequency the maximum insertion gain measured was 14 dB with L_g = 1.5 - 2.0 microns. The best noise figure was 4.2 dB with 6 dB associated gain measured on a 2 micron device. Included in this table are results obtained from NRL 5220 material, NRL Code 5212 ion implanted material, and industrial

material. Most of the material processed did not have a buffer layer. Note that all material reported in Table I is comparable in terms of N_D, a, doping slope and low field mobility. In addition, all material in Table I indicated a saturated drift velocity of $8.0\text{-}10.0\times10^6$ cm/sec. Maximum values of g_m were between 18 and 20 mmho and agree well with calculated values of g_m based on the NRL FET structure corrected for R_s. I_{DSS} ranged from 25 to 45 mA on best devices with the minimum noise figure occurring at $I_D=I_{DSS}/10$.

The results of Table I suggest a lower obtainable noise figure from industrial material with a buffer layer than from NRL material. However, the best results achieved using industrial material reported in Table I are more recent than those achieved with NRL 5220 material and reflect the improvement with time in the NRL processing technology. Recently, NRL LPE GaAs FET material has been supplied to an industrial laboratory with ½ micron gate fabrication technology. At 10 GHz a 3 dB noise figure with 10 dB associated gain was obtained on NRL material processed by this laboratory into ½ micron gate length FETs.

F. FET/Material Correlation

Although FET microwave performance varied from wafer to wafer, a conclusive relationship between materials properties and FET performance has not been deduced. Little is known about most of the semi-insulating substrates used for industrial material. All NRL 5220 LPE material employed non-converting Cr/Te doped semi-insulating substrates. The substrates used for NRL 5212 ion implanted FETs were obtained from Sumitomo Industries and did not

show surface conversion effects up to 900°C. Fig. 12 shows representative carrier concentration profiles for both NRL LPE and ion-implanted channel layers. The roll-off slope is between 600-800 Å/decade. Industrial material profiles resemble that of curve (1) in Fig. 12. Nearly all FETs fabricated from NRL 5220 material were processed prior to nondestructive characterization (NRL Code 5270) as a method of expediency in optimizing the 5220 LPE growth technology. The NRL LPE technology is now in hand and material is flowing through the nondestructive characterization portion of Fig. 1, but no definitive results are available at this writing. However, some general comments and observations can be made.

FETs fabricated from NRL LPE material showed almost no looping and absolutely no backside gating in darkness even when the backside gate potential was increased to 200 volts. Under microscope illumination a very small amount of backside gating can be observed. Virtually all of the industrial material shows some backside gating in darkness. However, there is no correlation between the presence of backside gating and FET performance since some of the better performing FETs have been made from material that showed considerable backside gating. The same can be said about looping. Some FETs showed looping at $I_D = I_{DS}$. The looping FETs performed as well as those FETs that did not loop. There was no crossing in any loop. FETs which were light sensitive performed as well as those which were not.

FETs made from NRL LPE material did show some variation in noise figure and gain, even when the doping profiles of the respective wafers were identical. Several wafers were grown with the doping profile (1) shown in Fig. 12 using Cr/Te substrates cut from the same boule. At 8 GHz the wafer to wafer variation in noise figure was as much as 6 dB while the DC characteristics, gate length and processing technology remained the same. This represents the most perplexing problem facing the FET industry today: GaAs material can look identical under most static characterization schemes but give dramatically different RF performance. It is hoped that the nondestructive characterization (photoluminescence and deep traps) can shed more light on this problem.

TABLE I

Wafer	N_D Doping Density	Channel Thickness	Interface Doping Slope	Average Channel Mobility	Pinch (V_P) Off Voltage	AC Trans-conductance (g_m)	Gate Length L_g	Minimum Noise fig. 8 GHz	Associated Gain 8 GHz
Number	cm^{-3}	Microns	Å/decade	cm^2/v.sec	Volts	mmho	Microns	dB	dB
NRL 5221 12-2gN LPE No buffer 4/77	$1.5x10^{17}$	0.25	700	3400	2.5-3.5	20 max. 15 avg. R_s=8 ohms	1.5	5.4	8
NRL 5212 Ion Imp. No buffer 8/77	$1.5x10^{7}$	0.25	700	3100	2.0-2.2	20 max. 18 avg. R_s=9.5 ohms	1.5	5.1	6
Industrial Vendor A VPE - No buffer 9/77	$9.5x10^{16}$	0.35	600	3600	4.0-5.0 recessed gate	18 max. 15 avg. R_s=6.5 ohms	2.0	4.3	6
Industrial Vendor B VPE buffer 9/77	$9.0x10^{16}$	0.22	600	3500	3.0-3.5	20 max. 16 avg. R_s=9.5 ohms	2.0	4.2	6
NRL 5221 12-78N LPE No buffer 8/77	$1.3x10^{17}$	0.30	600	3600	3.0-4.0	18 max. 12 avg. R_s=8 ohms	1.5	5.1	4

Note: Gate width = 250 microns all devices

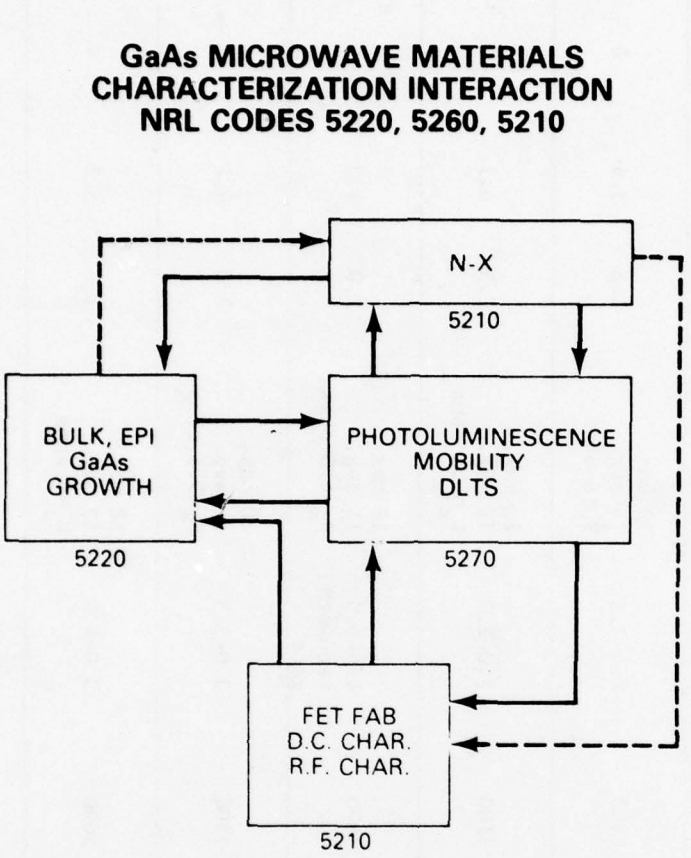

Fig. 30 — Block diagram representation of interdisciplinary effort on GaAs microwave materials characterization at NRL

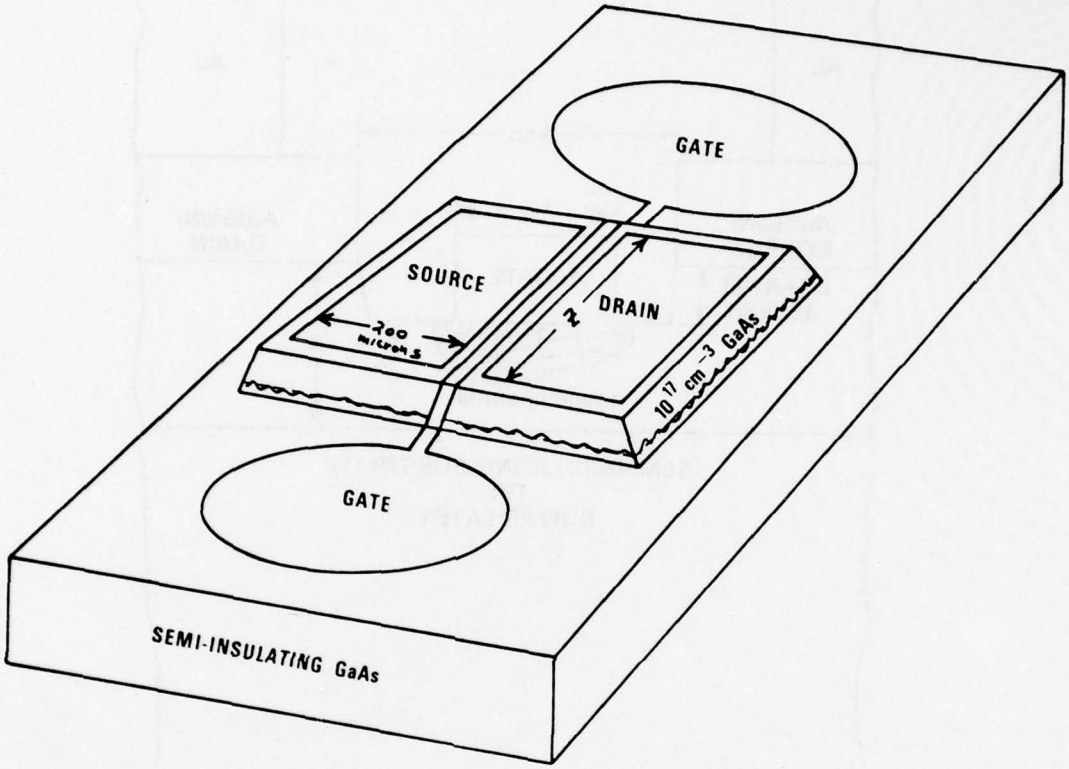

Fig. 31 — Schematic representation of NRL GaAs FET structure

AD-A053 308 NAVAL RESEARCH LAB WASHINGTON D C F/G 20/12
CHARACTERIZATION OF III-V MATERIALS. ANNUAL SUMMARY REPORT, 1 O--ETC(U)
FEB 78 B D MCCOMBE

UNCLASSIFIED NRL-MR-3701 NL

2 OF 2
AD
A053308

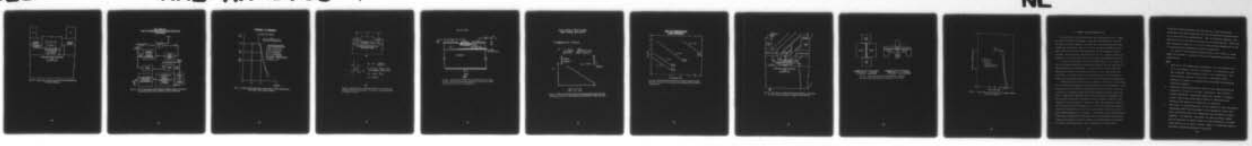

END
DATE
FILMED
6-78
DDC

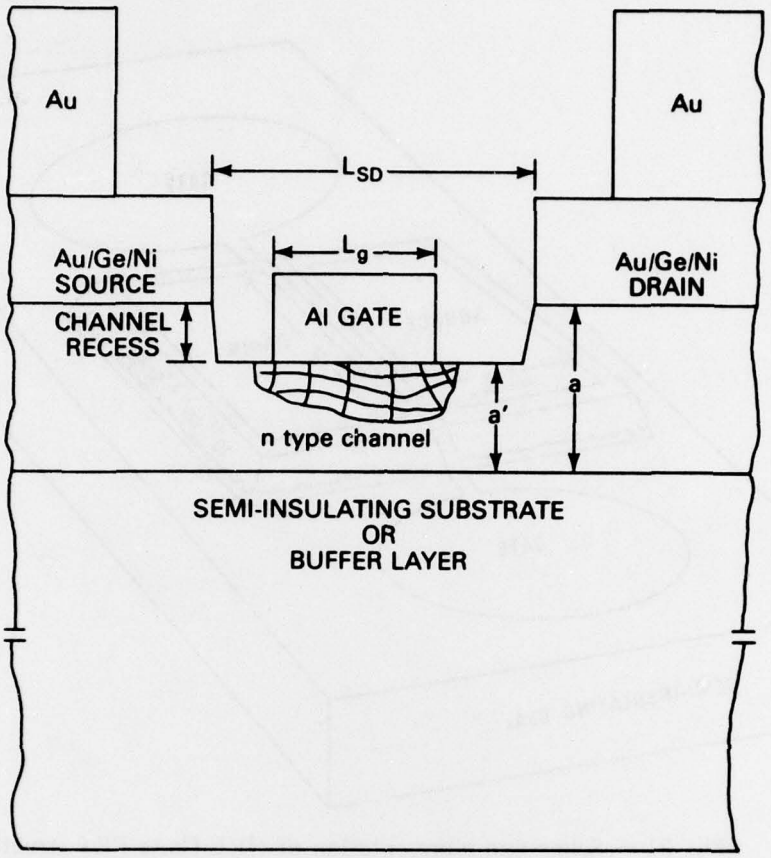

Fig. 32 — Cross section of NRL GaAs FET showing metallizations and key dimensions

NRL CODE 5211
GaAs FET FABRICATION AND CHARACTERIZATION
FLOW CHART

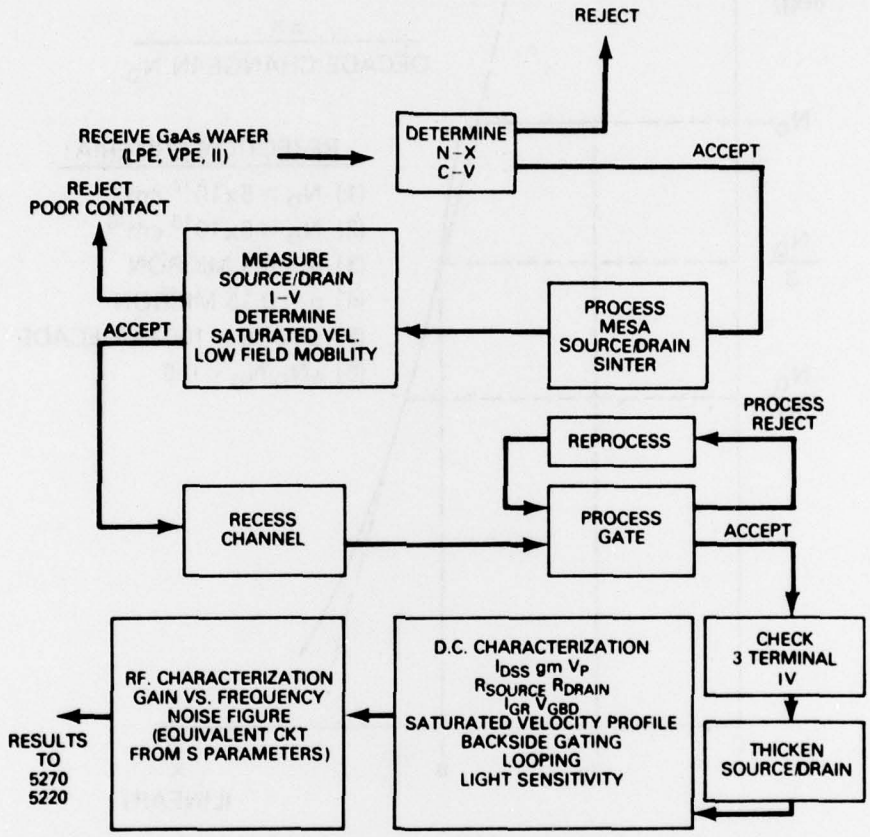

Fig. 33 — Flow chart showing GaAs material in different stages of processing and characterization done exclusively by NRL Code 5211S

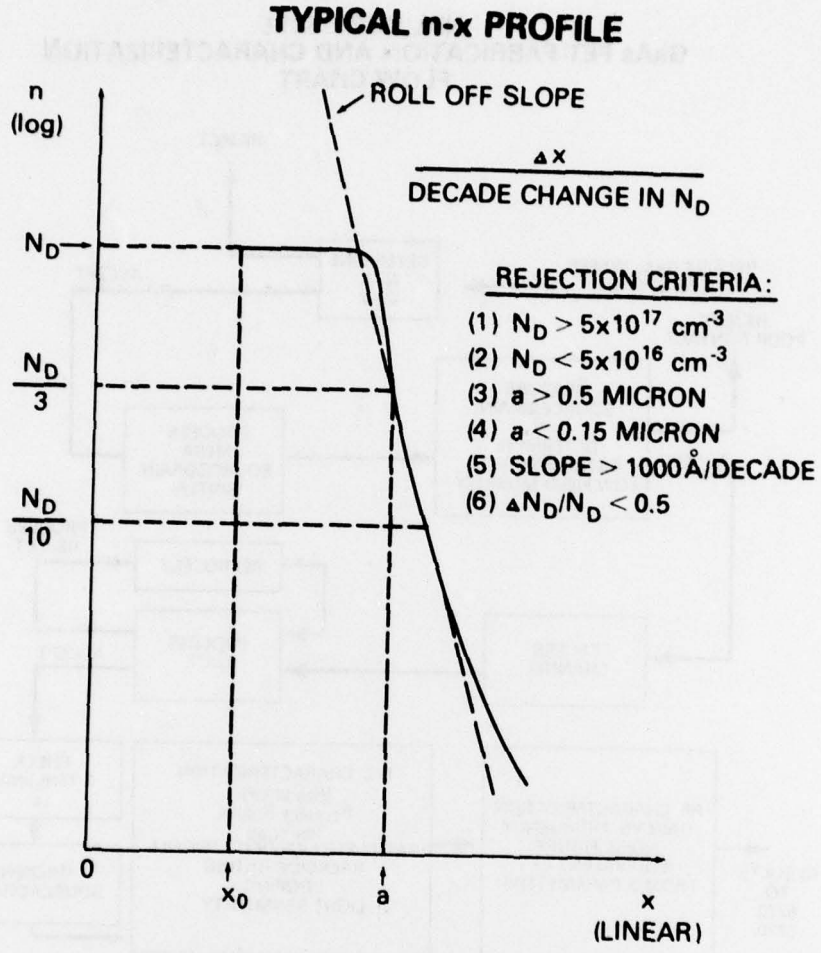

Fig. 34 — Typical carrier concentration versus distance profile obtained from C/V profiler. Note rejection criteria.

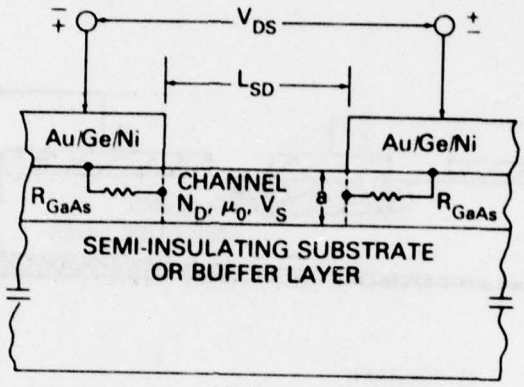

(a)

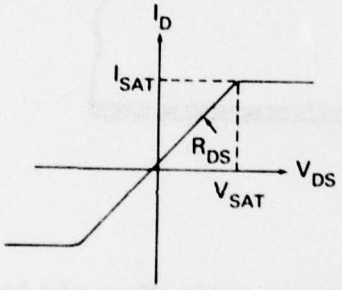

$$R_{DS} = 2R_C + \frac{L_{SD}}{qN_D \bar{\mu}_0 a Z}$$

$$R_C = R_{CONTACT} + R_{PROBE} + R_{GaAs}$$

(FOR SYMMETRIC STRUCTURE)

$$V_{SAT} \cong L_{SD}E_P + 2R_C I_{SAT}$$

$$I_{SAT} = q\bar{V}_S N_D a Z$$

(b)

Fig. 35 — Contact resistance and saturated drift velocity measurement performed before gate is in position. I/V curve plus equations are used to determine R_c and $\bar{V}_s$.

BACK SIDE GATING

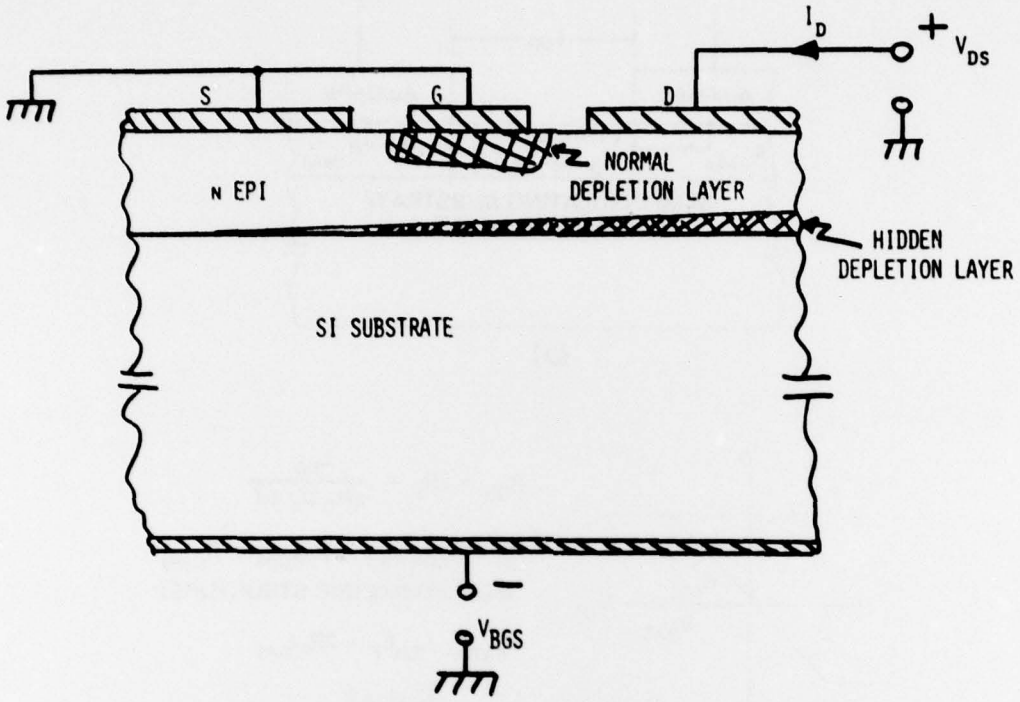

Fig. 36 — Experimental electrical setup for measuring effects of a back-side gate. The back gate potential modulates the extent of the hidden depletion region which in turn modulates I_D.

VARIAN TECHNIQUE OF PROFILING AVERAGE
CHANNEL SATURATED DRIFT VELOCITY

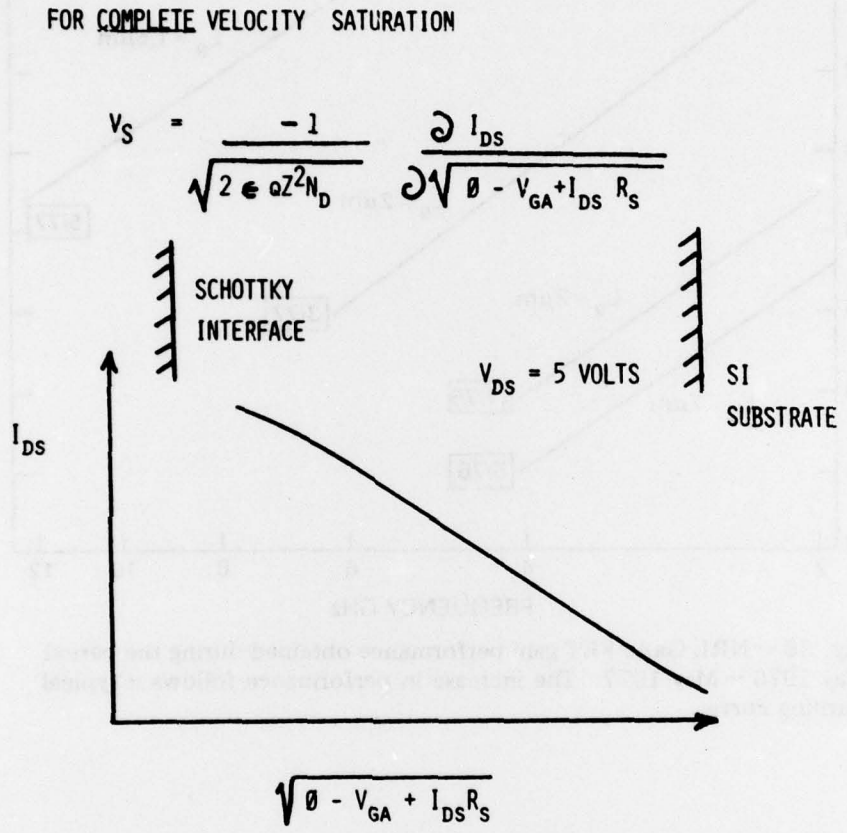

Fig. 37 — Method of determining $\overline{V}_S$ using experimentally measured DC parameters I_{DS}, V_g and R_s. This technique was developed by Varian Associates.

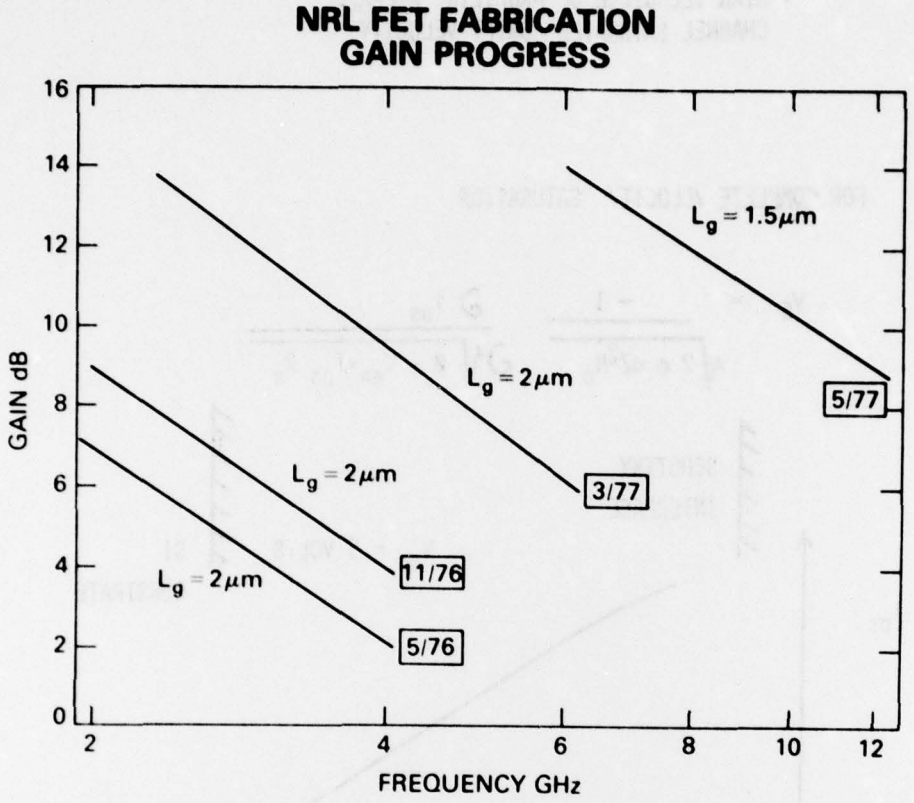

Fig. 38 — NRL GaAs FET gain performance obtained during the period May 1976 — May 1977. The increase in performance follows a typical learning curve.

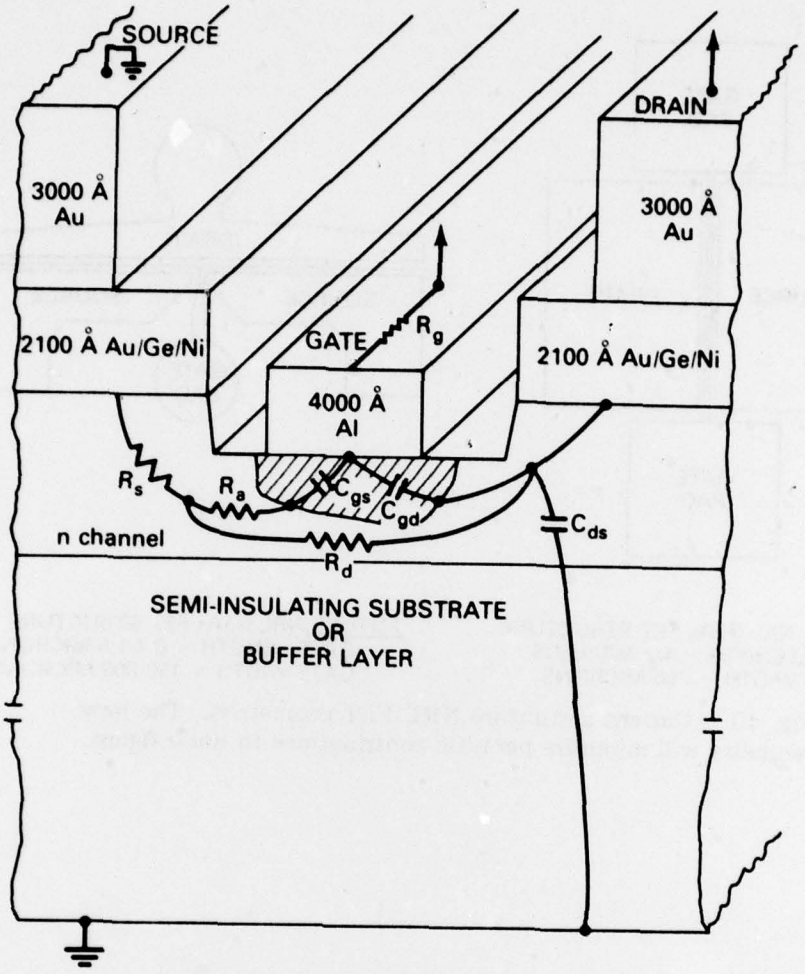

Fig. 39 — Cross section of NRT FET showing metallization thicknesses and key intrinsic and parasitic equivalent circuit elements

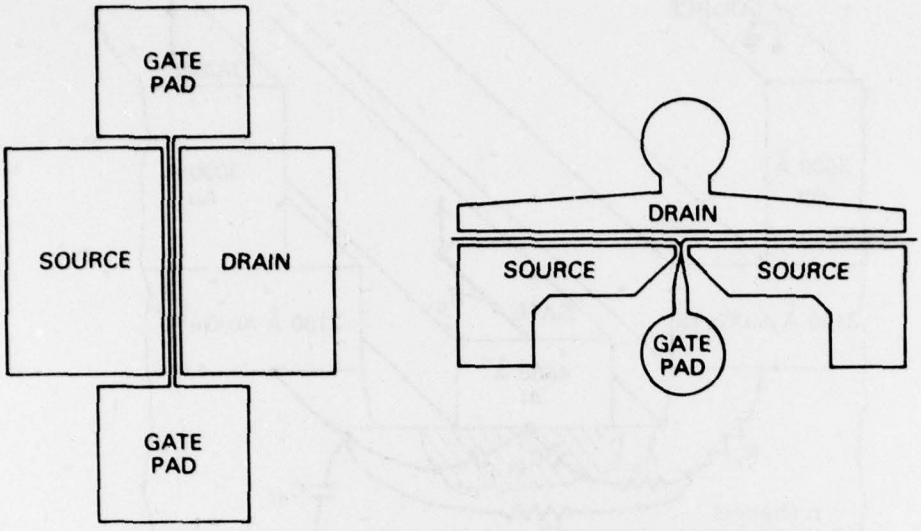

CURRENT NRL GaAs FET STRUCTURE
GATE LENGTH = 1-2 MICRONS
GATE WIDTH = 250 MICRONS

FUTURE NRL GaAs FET STRUCTURE
GATE LENGTH = 0.7-1.5 MICRONS
GATE WIDTH = 150-300 MICRONS

Fig. 40 — Current and future NRL FET geometries. The new geometry will minimize parasitic contributions to noise figure.

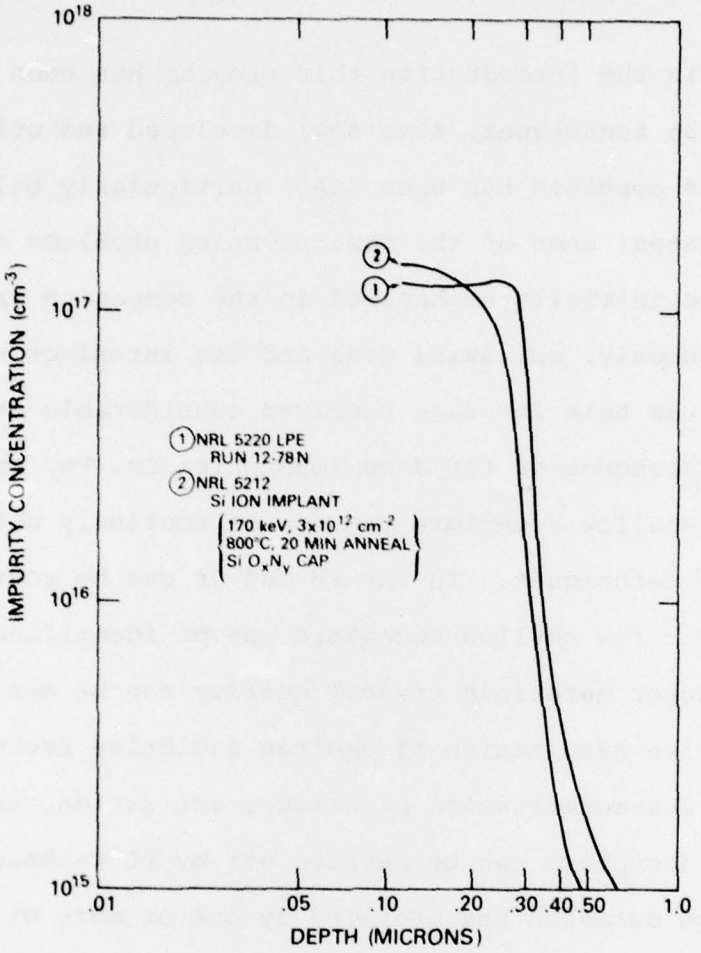

Fig. 41 — Typical LPE and ion implanted N/X profiles obtained on NRL FET material

V. SUMMARY AND RECOMMENDATIONS

As outlined in the introduction this program has seen a number of characterization techniques, some new, developed and utilized. The main materials emphasis has been GaAs, particularly bulk semi-insulating substrates; some of the most pressing problems existed here, and this was initially emphasized in the companion growth program. More recently, epitaxial GaAs and its interface with the substrate as well as bulk InP have received considerable attention.

In GaAs the presence of the deep impurities Cr, Fe, oxygen as well as numerous shallow acceptors can now be routinely detected by photoluminescence techniques. In InP Fe and Cr can be routinely detected but only a few shallow acceptors can be identified with certainty. For purer materials crystal quality can be estimated from high resolution examination of exciton radiative recombination.

Rudimentary characterization of damage, activation, and profiles of ion implanted acceptors can be carried out by PL techniques. Deep trap levels can be detected and profiled by one or more of several versions of transient capacitance spectroscopy which are now available. Temperature dependent Hall and resistivity measurements can be routinely utilized to determine carrier density, mobility, net impurity and total impurity concentrations, and activation energies for electrically active impurities. Contactless mobility measurements can be carried out for thin active n-type layers by a microwave magnetoconductivity technique. Contactless IR reflectivity and differential absorption techniques have been developed for probing lateral variations in carrier density and determining the presence of certain non-electrically active impurities, respectively.

Interface related problems for LPE layers on semi-insulating substrates have been recognized and can be partially characterized by PL and electrical measurements. The net majority impurity concentration can be profiled routinely by C-V measurements. FETs with gate lengths as small as 1 μm can be routinely processed and dc and rf characteristics measured for device evaluation.

In spite of considerable progress there still remain a large number of problems. Several of the most outstanding problems are listed below.

GaAs

1. Details of the compensation mechanism, e.g. the precise role of Cr and oxygen, are still incomplete. In particular, the NRL "undoped" semi-insulating GaAs is not understood. This understanding requires a concerted, coordinated effort employing a number of characterization methods and carefully controlled samples.
2. Commercial mass spectroscopic data for the identification of impurities in GaAs is, at best, unreliable. More careful studies employing a dedicated system are needed, or alternatively, some other quantitative means of identifying and measuring the density of impurities is required.
3. The cause of "type conversion" of the surface of semi-insulating substrates under heat treatment is not completely clear, and hence qualifying tests for substrates have no basis in understanding. In addition, the effect of type converted layers, and the efficacy of buffer layers on the performance of active layer devices is not well in hand. Again, a concerted study of carefully controlled samples is required.

4. A routine means of identifying donor impurities is required. High resolution far IR photoconductivity can be utilized in high quality, low impurity density ($< 10^{14} cm^{-3}$) samples, but not in higher density samples.
5. The effects of processing on material characteristics and device performance and reliability, and the separation of processing induced problems from inherent materials problems are not well characterized. An extensive effort is required to sort out these problems.
6. Ion implantation is a very promising technology for microwave device fabrication on GaAs. Considerable additional work in the area of understanding defects, encapsulation and annealing, electrical activation, etc., is required.

InP - Items 1-6 can be reiterated for InP noting that the level of understanding in each case is much lower. In addition, there are other problems that should be investigated.

7. For InP there is not a good data base for the identification of impurities. The necessary work, careful back doping and PL and other measurements, should be carried out to provide this data base.
8. Heat treatment is a particularly severe problem for InP since the surface degrades at a much lower temperature than that of GaAs, and no type conversion studies have been carried out.